

# Optical control of gene expression using a DNA G-quadruplex targeting reversible photoswitch

Received: 23 May 2024

Accepted: 4 March 2025

Published online: 03 April 2025

 Check for updates

Xiaoyun Zhang<sup>1</sup>, Somdutta Dhir<sup>2</sup>, Larry Melidis<sup>2</sup>, Yuqi Chen<sup>1</sup>, Zutao Yu<sup>1</sup>, Angela Simeone<sup>2</sup>, Jochen Spiegel<sup>1</sup>, Santosh Adhikari<sup>1</sup> & Shankar Balasubramanian<sup>1,2,3</sup> ✉

Transcriptional regulation is a dynamic process that coordinates diverse cellular activities, and the use of small molecules to perturb gene expression has propelled our understanding of the fundamental regulatory mechanisms. However, small molecules typically lack the spatiotemporal precision required in highly non-invasive, controlled settings. Here we present the development of a cell-permeable small-molecule DNA G-quadruplex (G4) binder, termed G4switch, that can be reversibly toggled on and off by visible light. We have biophysically characterized the light-mediated control of G4 binding *in vitro*, followed by cellular, genomic mapping of G4switch to G4 targets in chromatin to confirm G4-selective, light-dependent binding in a cellular context. By deploying G4switch in living cells, we show spatiotemporal control over the expression of a set of G4-containing genes and G4-associated cell proliferation. Our studies demonstrate a chemical tool and approach to interrogate the dynamics of key biological processes directly at the molecular level in cells.

The dynamic gene expression control is vital for regulating critical biological processes such as cell differentiation and development, and cellular homeostasis<sup>1</sup>. During these processes, genes are expressed at specific times and locations within cell populations<sup>2,3</sup>. Methods that enable spatiotemporal modulation of gene expression will help us elucidate gene regulatory mechanisms. Small molecules can be used to interrogate gene regulation<sup>4</sup>; however, they generally lack the high resolution for spatiotemporal control necessary in highly non-invasive and controlled applications. Photomodulation of biomolecular targets can enable spatiotemporal control with high precision, as exemplified by light-inducible transcriptional effectors<sup>5</sup>. Photocontrolled bioactive small molecules offer an approach that simplifies dosing and circumvents the genetic engineering required by the conventional optogenetics technique<sup>5–7</sup>. For example, photoswitchable inhibitors of histone deacetylase have provided optical control of the epigenetically regulated transcriptome<sup>8</sup>. Herein we introduce an approach for

reversible, spatiotemporal control of gene expression by manipulating DNA with light-responsive small molecules.

DNA G-quadruplexes (G4s) are four-stranded secondary nucleic acid structures formed by stacked G-tetrads, stabilized by centrally coordinated cations ( $M^+$ ) in a preference order of  $K^+ > Na^+ > Li^+$ , within certain guanine-rich genomic sequences<sup>9,10</sup> (Fig. 1a). DNA G4 structures have previously been identified in human cells<sup>11,12</sup>, and the dynamics of their formation have been visualized in live cells<sup>13</sup>. Recently, endogenous G4-forming sites have been mapped in human chromatin, showing their predominant localization in regulatory regions, particularly within active promoters of cancer genes<sup>14,15</sup>. These G4s have been shown to be highly correlated with transcriptional programmes across different breast cancer subtypes<sup>16</sup>. Furthermore, it has been demonstrated that G4 formation within gene promoters at specific loci, through site-specific G4 editing in human genome, can promote downstream gene transcription<sup>17,18</sup>. Notably, accumulating evidence

<sup>1</sup>Yusuf Hamied Department of Chemistry, University of Cambridge, Cambridge, UK. <sup>2</sup>Cancer Research UK Cambridge Institute, Li Ka Shing Centre, University of Cambridge, Cambridge, UK. <sup>3</sup>School of Clinical Medicine, University of Cambridge, Cambridge, UK. ✉e-mail: [sb10031@cam.ac.uk](mailto:sb10031@cam.ac.uk)

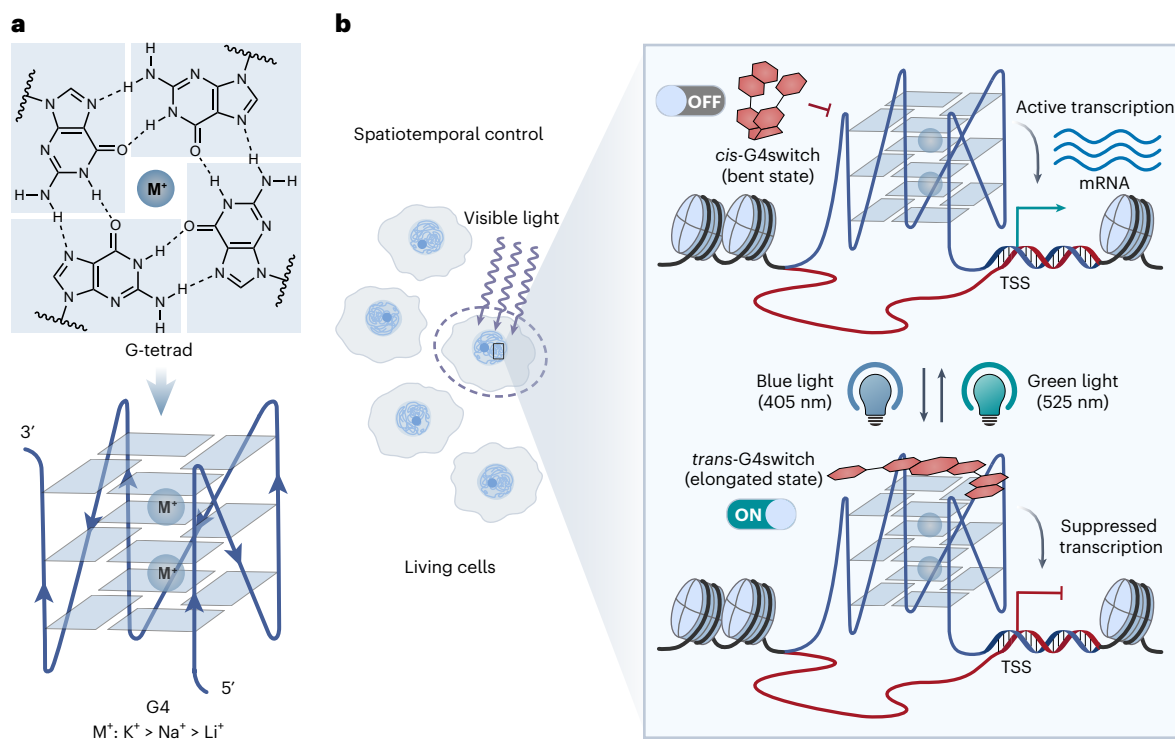


**Fig. 1 | Schematic for the optical control of gene expression by G4switch.**

**a**, A G-tetrad, comprising four Hoogsteen hydrogen-bonded guanines, stabilized by a central monovalent cation (top) following a preference order of potassium ( $K^+$ ) > sodium ( $Na^+$ ) > lithium ( $Li^+$ ), and a parallel intramolecular G4 structure composed of stacked G-tetrads (bottom). **b**, Schematic diagram for the concept

of optically controlling gene expression using a photoswitchable G4 ligand G4switch. Upon blue (405 nm) or green (525 nm) light illumination, G4switch can be switched 'ON' or 'OFF', respectively, in live cells to enable it to reversibly bind to endogenous DNA G4s and inhibit the gene expression, thus achieving spatiotemporal control of gene expression. TSS, transcription start site.

suggests that G4s can operate as binding hubs for transcription factors and the associated proteins<sup>19–21</sup>. However, the exact timing of G4 formation and how this is precisely linked to transcriptional regulation are still not fully understood<sup>22</sup>. Thus, understanding the mechanisms of G4-associated transcriptional regulation has become a significant challenge central to the field, underscoring the need for the development of tools to target folded G4s with high spatiotemporal precision. Several G4-selective small-molecule ligands have been shown to perturb gene expression<sup>23,24</sup>, but they lack the precision for highly non-invasive spatiotemporal control. Attempts at photoresponsive G4 ligands have shown limited applicability in biological contexts<sup>25–29</sup>, owing to a number of challenges that include lack of reversibility or insufficient difference in activity between two isomers, loss of efficacy in physiological conditions (for example, high  $K^+$  concentration), the low tissue penetration and the potential for causing cell phototoxicity upon ultraviolet (UV) light exposure<sup>30</sup>.

Herein we present a chemical approach to optically modulate transcription of G4-containing genes in situ. We developed a cell-permeable small-molecule G4 ligand that is photoswitchable, designated G4switch. Its elongated *trans* conformation exhibits considerably higher G4-binding affinity and selectivity, compared with the bent *cis* form, which we demonstrate in vitro and in cells. Upon illumination with low-intensity blue (405 nm) and green (525 nm) light, G4switch can undergo rapid *cis*-to-*trans* and *trans*-to-*cis* photoisomerizations, respectively. We demonstrate that activated G4switch predominantly localizes to promoter G4s in human, cellular chromatin and can modulate transcription. This enables the optical control of expression at hundreds of G4-containing genes and G4-associated cell proliferation with a high spatial and temporal resolution. Here we demonstrate that a DNA-targeting small molecule can be exploited for the reversible optical control of gene expression.

## Results

### Design and characterization of G4switch

We set out to design and construct a photoswitchable small molecule with differential binding to G4 DNA in the two conformational states. We reasoned that such a ligand would, in its 'active' state, selectively target DNA G4 structures and inhibit gene transcription in living cells, enabling spatiotemporal control of G4-containing gene expression (Fig. 1b). We selected diazocine as the photoswitching moiety, owing to its well-characterized photothermal properties, a large geometrical difference between its bent *cis* and elongated *trans* isomers, and visible light-controlled photoisomerization in both directions<sup>31–33</sup> (Fig. 2a). We designed our G4switch probes by tethering a key G4-binding moiety 4-(2-aminoethoxy)quinolin-2-amine (blue), derived from a widely used small-molecule G4 ligand pyridostatin (PDS)<sup>34</sup>, and a lipophilic positively charged nitrogen heterocycle group (red), derived from a potent G4 ligand of the pyridine-2,6-dicarboxamides (PDCs)<sup>35,36</sup>, to a diazocine core (teal) for reversible photoswitching (Fig. 2b,c). Given that small-molecule G4 ligands typically necessitate a flat aromatic skeleton for  $\pi$ -stacking with G-tetrads<sup>37</sup>, our design rationale was that such ligands could much more efficiently stack on the G-tetrad of G4s in the elongated *trans* form, which is closer to a planar conformation, compared with the bent *cis* form.

To identify a suitable photoswitchable ligand of this structural class, we synthesized a series of putative G4switches (**1–10**) by amide and Suzuki–Miyaura coupling, in two to three steps from known building blocks **S1** and **S2** (Fig. 2c and Supplementary Information). Given the importance of cell permeability of probes for explorations in living systems, we first calculated the theoretical physicochemical properties of all compounds and assessed them with the 'Lipinski's rule of five' (Extended Data Fig. 1a), which is widely used as a guideline for drug-likeness<sup>38</sup>. Compared with the parent molecule PDS, we observed

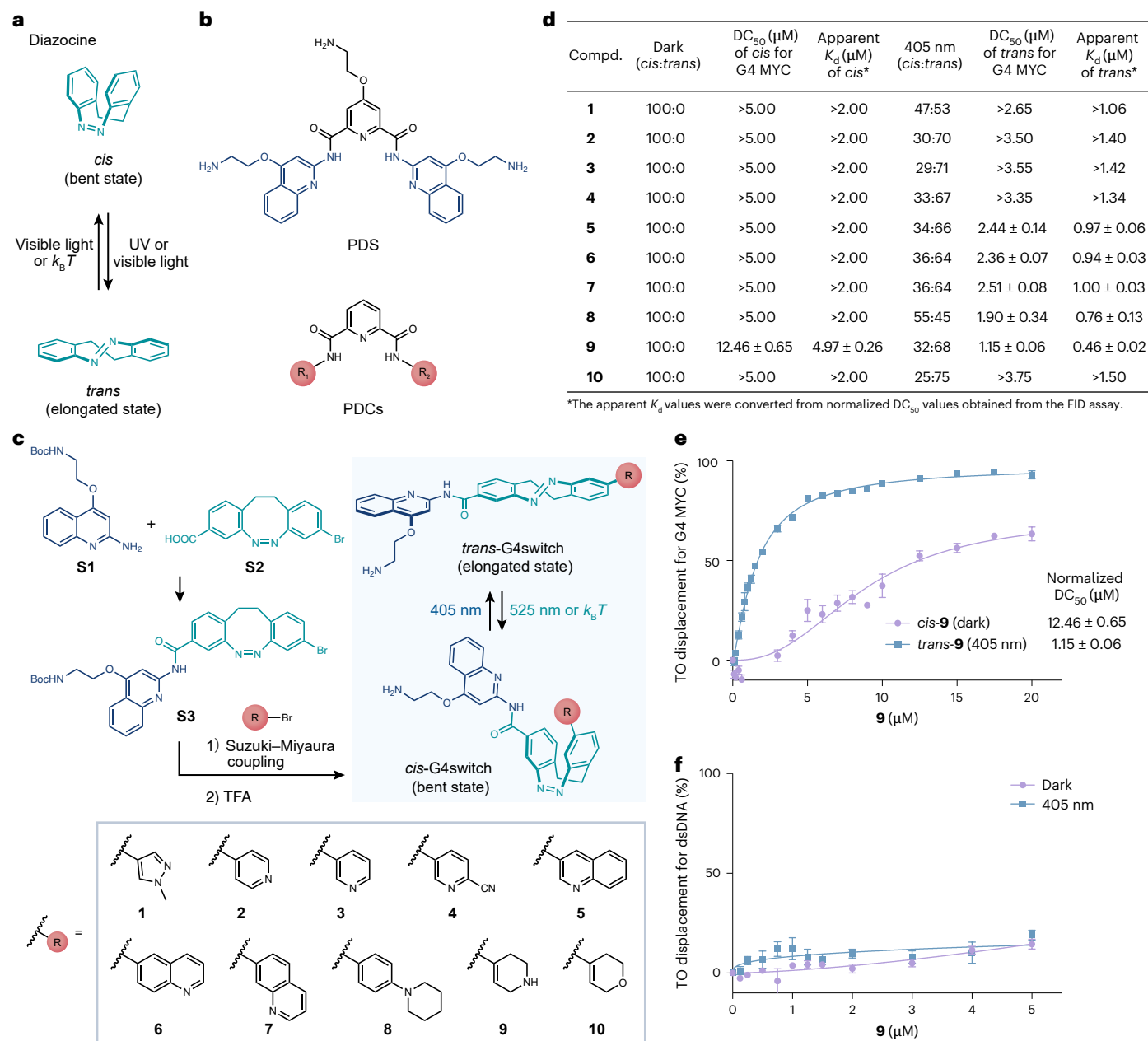


**Fig. 2 | Design, synthesis and screening of the G4switch. a**, Diazocine photoisomerization. **b**, Chemical structures of PDS and PDC scaffold. R<sub>1</sub> and R<sub>2</sub> represent *N*-heterocycles. **c**, Synthesis and photoswitching of the putative G4switches. TFA, trifluoroacetic acid. **d**, Summary of *cis:trans* ratios of putative G4switches in the dark and following 405 nm illumination in DMSO, as determined by <sup>1</sup>H NMR spectroscopy at room temperature (Supplementary Fig. 1), and their normalized DC<sub>50</sub> values, the concentrations of the corresponding isomers required to achieve a 50% decrease in fluorescence upon competitive

displacement of a fluorescent G4 binder TO from a G4 MYC structure, obtained from the FID assay, as well as the apparent K<sub>d</sub> values derived from the normalized DC<sub>50</sub> values and the association rate constant (K<sub>a</sub>) of TO with G4 MYC (Methods). The FID results are shown as mean ± s.d. from three or four technical replicates (n = 3 for **9**; n = 4 for the other molecules). **e, f**, FID curves showing the percentage of displacement of TO for increasing concentrations of **9** from G4 MYC (**e**) (n = 3) and dsDNA (**f**) (n = 4) before and after 405 nm illumination.

considerable improvements for all compounds, which obey most of the properties in the rule. Furthermore, we determined the photoswitching properties of all compounds using <sup>1</sup>H NMR spectroscopy (Fig. 2d and Supplementary Fig. 1). As expected, the selected 3,3'-disubstituted diazocine moiety enabled rapid and reversible photoisomerization for all molecules in dimethyl sulfoxide (DMSO) controlled by visible light (405 nm and 525 nm)<sup>33</sup>: without illumination, we exclusively obtained the thermodynamically more stable *cis* isomers, which could be switched to the *trans* state by 405 nm illumination, reaching the photoisomerization ratios of up to 75% of the *trans* isomer (Fig. 2d and Supplementary Fig. 1).

We then assessed the G4-binding affinity and selectivity of putative G4switches towards G4 structures before and after 405 nm illumination using a well-established fluorescent intercalator displacement (FID) assay<sup>39,40</sup>. Specifically, we evaluated the ability of the putative ligand to competitively displace a known fluorescent G4 binder, thiazole orange (TO), from a folded DNA G4 MYC structure (Extended Data Fig. 1b), by measuring a decrease in fluorescence (DC<sub>50</sub>)<sup>39</sup> (Fig. 2d,e and Supplementary Fig. 2), which were converted to the binding constant (K<sub>d</sub>) of ligands as previously reported<sup>40</sup> (Fig. 2d and Methods). Compounds **5–9** all show a clear difference in apparent G4-binding affinity between their *cis* and *trans* isomers, with at least 2-fold selectivity, while others

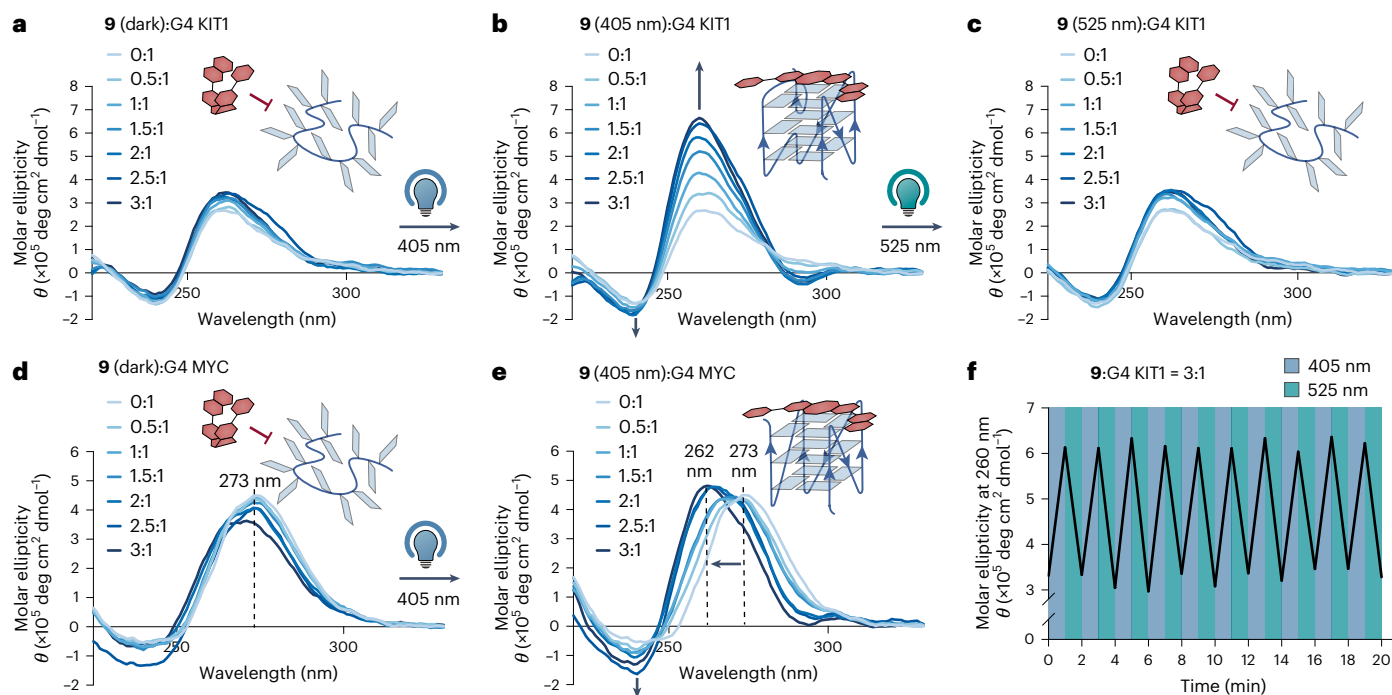


**Fig. 3 | Characterization of light-dependent G4-binding activity of G4switch in vitro.** **a–e**, CD spectra of 10 μM G4 KIT1 (**a–c**) and G4 MYC (**d,e**) collected by titrating with increasing amounts of **9** in 10 mM Tris-HCl buffer, 100 mM LiCl, pH 7.4 before (**a,d**) and after (**b,e**) 405 nm illumination for 60 s, and further (**c**)

525 nm illumination for 60 s. **f**, G4 KIT1 (10 μM) formation, indicated by the CD intensity measured at 260 nm, in the presence of 3 molar equivalents of **9**, is rapidly and reversibly photoswitched in 10 mM Tris-HCl buffer, 100 mM LiCl, pH 7.4, by alternating phases of 405 nm and 525 nm illuminations.

showed negligible G4 binding in either state (Fig. 2d,e and Supplementary Fig. 2). Compound **9**, where R is 1,2,3,6-tetrahydropyridine, showed the largest change in G4-binding affinity, with the lowest apparent  $K_d = 0.46 \pm 0.02 \mu\text{M}$  for the 405 nm illuminated *trans* isomer, and about 10-fold lower G4-binding affinity (apparent  $K_d = 4.97 \pm 0.26 \mu\text{M}$ ) for the non-illuminated *cis* isomer (Fig. 2d,e). In addition, both isomers of **9** showed no apparent binding to a double-stranded DNA (dsDNA) control (Fig. 2f and Extended Data Fig. 1b). On substituting the basic secondary amine group, compound **10** is incapable of binding to G4s, for either isomer (Fig. 2d and Supplementary Fig. 2i), therefore suggesting that the electrostatic interactions between the positively charged secondary amine group of **9** and the negatively charged phosphate backbone of G4 DNA are critical<sup>37</sup>. Overall, our assay reveals that compound **9** is the most potent photoswitchable G4 ligand, exhibiting the highest G4 selectivity between its *cis* and *trans* forms.

Next, we pursued a more detailed characterization of **9**. The photoswitching of **9** was demonstrated in phosphate buffered saline (PBS) by UV–visible spectroscopy (Extended Data Fig. 2a–f). The data confirmed that 405 nm and 525 nm are the ideal photoswitching wavelengths, enabled by the 3,3′-disubstituted diazocine<sup>33</sup> (Extended Data Fig. 2a). The *cis*–*trans* photoisomerization is rapid and fully reversible by establishing its steady states of photoisomerizations under 405 nm and 525 nm illuminations within ~60 s, without observable degradation of the compound after several cycles (Extended Data Fig. 2b–d). In the dark, a spontaneous, thermally driven *trans*-to-*cis* isomerization of **9** generates 100% *cis* isomer, with half-lives ( $t_{1/2}$ ) of 11.2 h and 2.6 h at 25 °C and 37 °C, respectively (Extended Data Fig. 2e,f). This relatively fast reversal mechanism largely confines the bioactivity of activated **9** to 405 nm illuminated sites, as it reverts to its inactivated *cis* form at physiological temperatures within a few hours and would do so when it diffuses into non-illuminated regions.

To evaluate the ligand’s capacity to stabilize G4 structure formation, we carried out a titration experiment with **9** monitored by circular dichroism (CD) spectroscopy using two G4 DNA oligonucleotides G4

KIT1 and G4 MYC in the presence of  $\text{Li}^+$  ions, which do not favour G4 formation<sup>41,42</sup>. The CD spectrum of G4 KIT1, in the absence of **9**, exhibits a broad positive band at ~260 nm and a negative band at ~240 nm (Fig. 3a), consistent with the formation of a parallel G4 structure<sup>43</sup>. Upon titration with increasing amounts of **9** in the absence of 405 nm illumination, we observed very little spectral changes for G4 KIT1 (Fig. 3a,c), whereas upon illumination of **9** at 405 nm, we observed a substantial increase in ellipticity at the characteristic G4 bands (Fig. 3b and Supplementary Fig. 3a). For G4 MYC in  $\text{Li}^+$  buffer, we observed a positive band at ~273 nm and a broad negative band at 240–250 nm in the absence of **9** (Fig. 3d), which is not characteristic of any known G4 topology. In the presence of in situ activated **9**, the positive band shifted from ~273 nm to ~260 nm, with increased negative ellipticity at ~240 nm (Fig. 3e and Supplementary Fig. 3b), suggestive of parallel G4 formation<sup>43</sup>, whereas only a slight shift was observed with at least three molar equivalents of inactivated **9** (30 μM, where there will be some G4 binding given its apparent  $K_d = 4.97 \pm 0.65 \mu\text{M}$  measured in  $\text{K}^+$  buffer, as shown in Fig. 2d,e) (Fig. 3d and Extended Data Fig. 2g). Taken together, this demonstrates stabilization of parallel G4 structures by the *trans*-**9**, but not the *cis* isomer. Importantly, G4 stabilization by **9** was shown to be fully reversible after at least 10 complete cycles of photoswitching, without any noticeable efficiency loss (Fig. 3f). Our CD spectroscopy data confirm the robustness of **9** as a photoswitchable G4 ligand.

### Mapping the binding sites of **9** in cells upon light exposure

Next, we sought to determine whether **9** can bind to folded genomic G4 structures inside cells in a light-dependent manner. We used Chem-map methodology, which enables in situ mapping of binding sites for biotin-tethered chromatin-interacting small molecules<sup>44–46</sup>. This involves the recruitment of a transposase (Tn5) to a biotin tag covalently attached to small molecules, which allows for the site-selective introduction of next-generation sequencing adapters (Fig. 4a).

We first synthesized a biotinylated probe, G4switch-biotin, featuring a long PEG4 spacer to minimize potential steric effects on

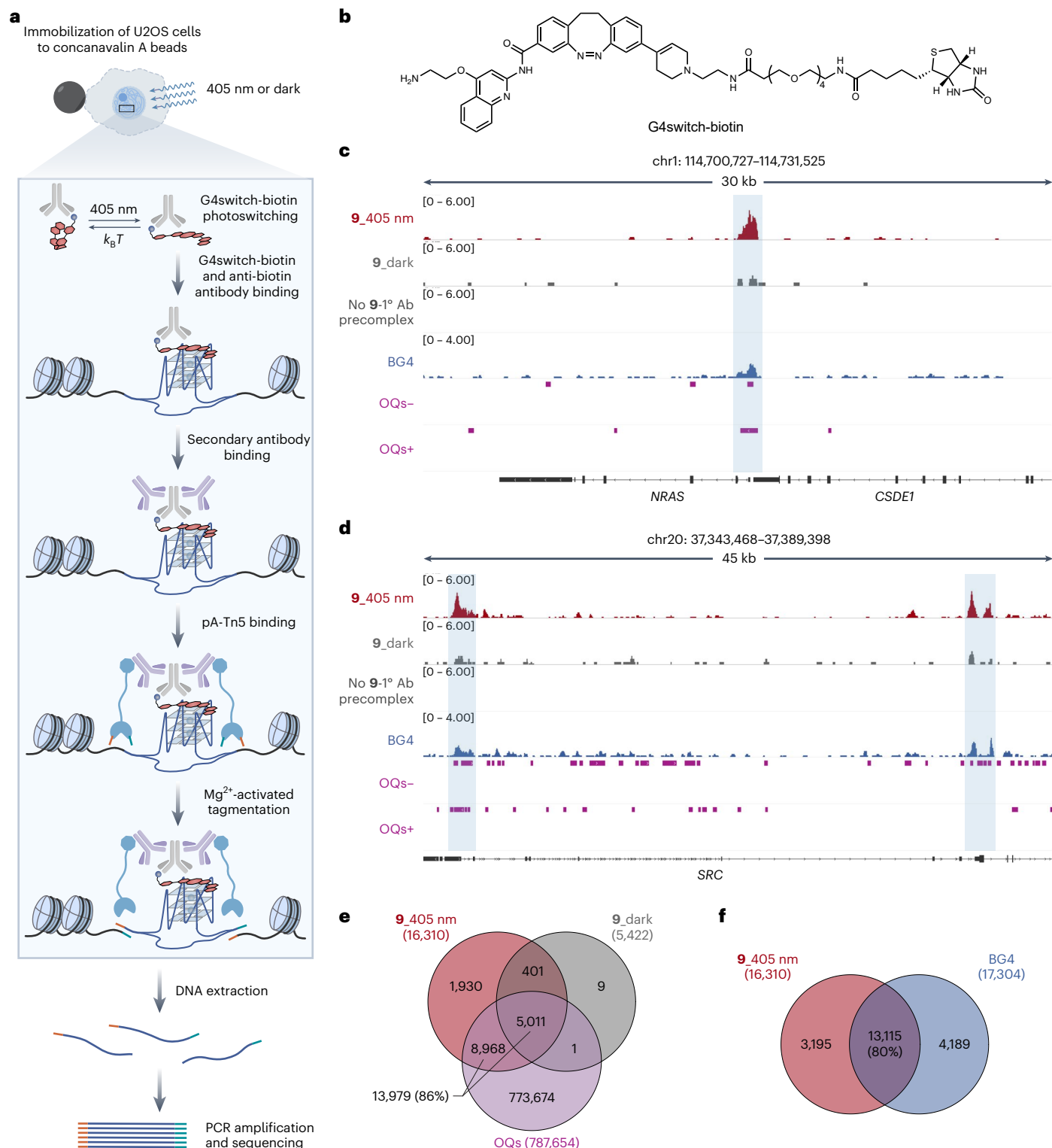


**Fig. 4 | Genome-wide profiling of G4switch binding sites in human cells.**

**a**, Schematic workflow of the G4switch-biotin Chem-map in U2OS cells. In permeabilized cells with or without 405 nm illumination, a precomplex comprising biotinylated **9** (red orange and blue) and anti-biotin antibody (grey) binds to DNA targets of **9**, followed by a sequential secondary antibody (purple) binding and a fusion transposome pA-Tn5 (light blue) binding to the target sites. Mg<sup>2+</sup> was then used to activate the Tn5 transposase in situ for DNA cleavage and sequencing adapter (orange and teal) integration adjacent to the **9** binding sites. After DNA isolation, PCR amplification of the fragments labelled with adapters at both ends generated the library, which was sequenced to identify the genomic binding sites of **9**. **b**, Chemical structure of G4switch-biotin. **c,d**, Genome browser

views of Chem-map binding sites of **9**, highlighted in light blue, in the presence (red) and absence (dark grey) of 405 nm illumination, and the negative control without adding G4switch-biotin-primary antibody precomplex (no **9**-1° Ab), compared with sites mapped by G4-CUT&Tag using G4-selective antibody BG4 (blue) at the *NRAS* (**c**) and *SRC* (**d**) loci, and G4 formation sites identified by G4-seq in both reverse (-) and forward (+) strand (purple). **e,f**, Venn diagrams showing the overlap of high-confidence binding sites between *trans*-**9**, *cis*-**9** and OQs (**e**), and between *trans*-**9** and BG4 (**f**). Chem-map experiments for both isomers of **9** were performed in three biological replicates, each with three technical replicates.

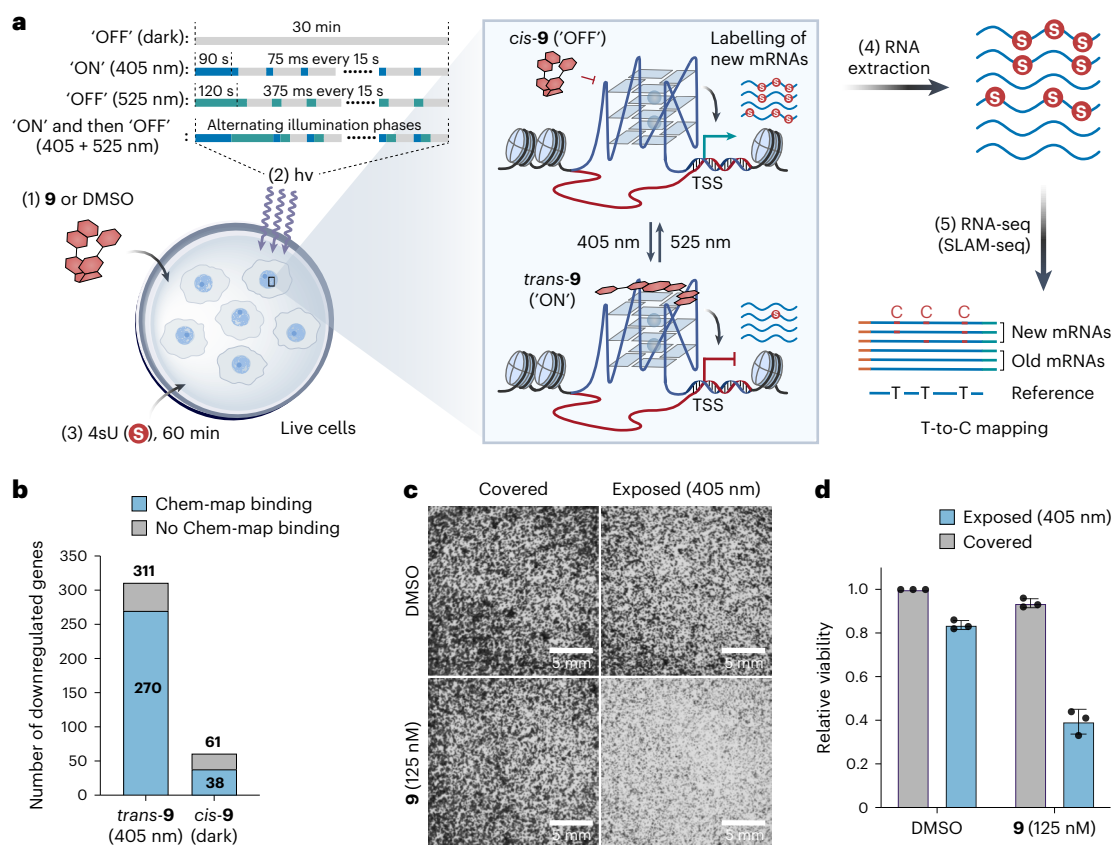


**Fig. 5 | G4switch optically controls transcription in living cells. a**, Schematic workflow of G4switch-mediated optical control of G4-containing gene expression profiled by SLAM-seq. U2OS cells were treated with **9** or DMSO control for 30 min in the dark or under indicated illumination conditions, followed by 4sU labelling over 60 min. RNA was extracted, and the abundance of newly synthesized RNAs was quantified by analysing T > C conversions through the SLAM-seq protocol. **b**, Stacked bar plot showing the overlap of downregulated genes by *trans-9* (upon 405 nm illumination) and *cis-9* (in the dark) with the corresponding Chem-map sites. Genes with Chem-map binding sites are shown in blue, while genes without Chem-map binding signals are

shown in grey. Four independent biological replicates were performed. **c**, Images showing light-dependent spatial control of U2OS cell proliferation with **9** compared with DMSO control within the same 6-well plate. Half of the plate was covered with a black mask before pulsed 405 nm illumination for 72 h, followed by crystal violet staining and imaging. Representative images from one out of three independent biological replicates with similar results are shown. **d**, Bar plot showing quantification of cell viability relative to DMSO treatment in the dark from **c**. Results are shown as mean  $\pm$  s.d. from three independent biological replicates ( $n = 3$ ).

**9**-target interactions (Fig. 4b). Using the FID assay, we confirmed that G4switch-biotin retains light-dependent G4-binding affinity and selectivity with an apparent  $K_d = 0.63 \pm 0.02 \mu\text{M}$  towards G4 MYC only in *trans* state, but not for dsDNA (Extended Data Fig. 3a). To distinguish binding profiles of *cis*- and *trans-9*, we performed the Chem-map experiments in permeabilized human osteosarcoma U2OS cells in the presence or absence of a 405 nm light source (Fig. 4a). We identified 16,310 high-confidence binding sites in the genome for *trans-9*, whereas a much smaller number of binding sites (5,422) were observed for the *cis-9* (Fig. 4c–e), of which nearly all (5,412/5,422) were a subset of *trans-9* binding sites (Fig. 4e). This is consistent with the relatively higher binding affinity of *trans-9* than the *cis* isomer for G4s (Fig. 2d,e). We carried out an analysis of differential binding sites<sup>47</sup> for both isomers of **9** and also evaluated the fraction of all mapped sequencing reads that fall into the called binding peak regions (FRIP, a quantitative measure of signal in each binding peak) for binding sites of both isomers of **9**, and the data confirmed substantially stronger and more frequent on-target binding of the *trans* isomer compared with the *cis* form (Extended Data Fig. 3b,c). A comparison of binding sites of *trans-9* in the genome with the previously observed universe of possible G-quadruplexes (OQs) detected in purified human genomic DNA by G4 sequencing (G4-seq)<sup>48</sup> showed high overlap (86%, 13,979/16,310) (Fig. 4e). Furthermore, we mapped 17,306 high-confidence endogenous folded G4 sites in U2OS

cells by G4-CUT&Tag using a G4-specific antibody BG4 (ref. 49). The majority of *trans-9* binding sites (80%, 13,115/16,310) overlapped with endogenous, folded G4s (Fig. 4f). In a competition experiment, we pre-incubated live U2OS cells with a competing G4-binding molecule, PDS (4  $\mu\text{M}$  and 20  $\mu\text{M}$ ), for 3 h before mapping the binding of **9** using Chem-map, in the presence of 405 nm illumination. Compared with a DMSO control, we observed substantial dose-dependent competition for *trans-9* binding events by PDS (293 and 6,227 significantly changing sites for 4  $\mu\text{M}$  and 20  $\mu\text{M}$  PDS treatment, respectively), as judged by differential binding analysis<sup>47</sup> (Extended Data Fig. 3d,e). These data suggest that light-activated *trans-9* engages at G4 DNA structures in cellular chromatin, while *cis-9* shows binding to fewer genomic G4 sites, consistent with its relatively weaker G4-binding affinity.

### Reversible optical modulation of gene expression in live cells

Formation of endogenous G4s in gene promoters has been linked to active transcription<sup>14,17,18</sup>. Treatment with G4-stabilizing molecules can potentially alter gene expression, by interfering with transcription machinery or transcription factor binding<sup>24,50</sup>. We therefore evaluated whether DNA G4 targeting by light-activated **9** could modulate the expression of genes, where G4s are targeted, in living cells.

We quantified immediate changes in transcription using a nascent RNA detection method called SLAM-seq<sup>51,52</sup>. We deployed a custom

illumination system to light-activate **9** in cultured cells (Supplementary Fig. 4). We subjected U2OS cells to a 30 min treatment with **9** (6  $\mu$ M) under either 405 nm illumination, control light illuminations or in the dark (Fig. 5a and Extended Data Fig. 4a,b). We then performed SLAM-seq to quantify changes in nascent RNA transcripts compared with an unilluminated DMSO treatment control (Fig. 5a). We observed that in situ light-activated *trans*-**9** significantly downregulated 311 genes (fold change  $>2$ ,  $q < 0.05$ ) (Fig. 5b, Extended Data Fig. 4c,d, Supplementary Fig. 5 and Supplementary Data 1). Notably, 87% (270/311) of these genes have *trans*-**9** binding sites as judged by Chem-map (Fig. 5b, and Extended Data Figs. 4e and 5). These observations are consistent with the hypothesis that targeting G4s with small molecules can reduce transcription<sup>24,50</sup>. By contrast, inactivated *cis*-**9** affected 80% fewer genes (61 genes), with reduced *cis*-**9** Chem-map binding signals (38/61) (Fig. 5b and Supplementary Data 1). This suggests that *trans*-**9** binding has a substantial direct impact on transcription, whereas the weaker G4-binding *cis*-**9** has a smaller effect. Interestingly, the expression levels of most (68%, 210/311) *trans*-**9** altered genes were ‘rescued’ by cycles of reversal of **9** (Extended Data Fig. 4d, Supplementary Fig. 6a and Supplementary Data 1). These data show potential for **9** to control gene expression under reversible control using light.

Stabilization of endogenous DNA G4 structures by G4-selective small molecules can inhibit gene expression and has shown good activity against cancer cell lines<sup>23,24</sup>. To exemplify spatial control using **9**, we grew U2OS cells in the same 6-well plate in the presence of **9** (125 nM) or vehicle DMSO for 72 h, activated the molecule with pulsed 405 nm illumination (60 s continuous illumination followed by pulses of 75 ms every 22.5 s) of half of the respective wells and quantified differences in cell density (Fig. 5c,d and Supplementary Fig. 7). We observed a clear inhibition of cell proliferation ( $<40\%$  relative viability) that is conditional on **9** treatment and 405 nm light exposure, while 405 nm light in the absence of **9** or **9** without light showed negligible effects (Fig. 5c,d). Consistent with a previous study<sup>23</sup>, we observed activation of the cellular DNA damage marker  $\gamma$ H2AX upon incubation with 405 nm light-activated **9**, its parent molecule PDS, and camptothecin, a DNA topoisomerase I inhibitor (Extended Data Fig. 4f). In the U2OS cell line, after 72 h of treatment with both G4 ligands (activated **9** and PDS), we did not observe apoptosis, as measured by PARP1 cleavage, unlike with camptothecin (Supplementary Fig. 8), indicating that 405 nm light-activated **9** behaves similarly to PDS, but differently from camptothecin, causing antiproliferative effects rather than cell death. These results confirm the spatial, light-mediated control of **9** action on cell antiproliferation, induced by DNA damage response.

## Discussion

We have designed and validated a small-molecule G4-targeting photoswitchable ligand. The G4switch, **9**, is a chemical tool capable of binding and stabilizing DNA G4s in human cells with reversible, spatiotemporal control. Using a variety of biophysics and cellular genomic approaches, we demonstrated that the ‘ON’ and ‘OFF’ conformations have considerably different affinities and stabilization capacities towards G4s. The activated *trans*-**9** maps strongly to endogenous G4 structures in human chromatin, relative to the inactivated *cis* form, and causes inhibition of genes proximal to the mapped binding sites of **9**. Importantly, the activation of G4switch in living cells is fully biocompatible using only visible light and can be easily reversed to the ‘OFF’ *cis* form. Notably, we have shown that **9** can be used to reversibly modulate the expression of several oncogenes, such as *FOS* and *JUN* (Supplementary Fig. 6b). This may provide ways to elucidate role of cancer-related gene regulation mechanisms through G4-mediated control.

Given that the dynamics of G4 formation have been implicated in a wide range of critical biological processes<sup>10</sup>, such as DNA replication, cancer biology and cellular differentiation<sup>53</sup>, we envisage that there is scope to exploit the spatiotemporal control of G4switch molecule **9** to explore such processes in the future.

## Online content

Any methods, additional references, Nature Portfolio reporting summaries, source data, extended data, supplementary information, acknowledgements, peer review information; details of author contributions and competing interests; and statements of data and code availability are available at <https://doi.org/10.1038/s41557-025-01792-1>.

## References

- Hager, G. L., McNally, J. G. & Misteli, T. Transcription dynamics. *Mol. Cell* **35**, 741–753 (2009).
- Buxbaum, A. R., Haimovich, G. & Singer, R. H. In the right place at the right time: visualizing and understanding mRNA localization. *Nat. Rev. Mol. Cell Biol.* **16**, 95–109 (2015).
- Moses, L. & Pachter, L. Museum of spatial transcriptomics. *Nat. Methods* **19**, 534–546 (2022).
- Schneider-Poetsch, T. & Yoshida, M. Along the central dogma—controlling gene expression with small molecules. *Annu. Rev. Biochem.* **87**, 391–420 (2018).
- Konermann, S. et al. Optical control of mammalian endogenous transcription and epigenetic states. *Nature* **500**, 472–476 (2013).
- Hüll, K., Morstein, J. & Trauner, D. In vivo photopharmacology. *Chem. Rev.* **118**, 10710–10747 (2018).
- Emiliani, V. et al. Optogenetics for light control of biological systems. *Nat. Rev. Methods Prim.* **2**, 55 (2022).
- Reis, S. A. et al. Light-controlled modulation of gene expression by chemical optoepigenetic probes. *Nat. Chem. Biol.* **12**, 317–323 (2016).
- Sen, D. & Gilbert, W. Formation of parallel four-stranded complexes by guanine-rich motifs in DNA and its implications for meiosis. *Nature* **334**, 364–366 (1988).
- Varshney, D., Spiegel, J., Zyner, K., Tannahill, D. & Balasubramanian, S. The regulation and functions of DNA and RNA G-quadruplexes. *Nat. Rev. Mol. Cell Biol.* **21**, 459–474 (2020).
- Biffi, G., Tannahill, D., McCafferty, J. & Balasubramanian, S. Quantitative visualization of DNA G-quadruplex structures in human cells. *Nat. Chem.* **5**, 182–186 (2013).
- Henderson, A. et al. Detection of G-quadruplex DNA in mammalian cells. *Nucleic Acids Res.* **42**, 860–869 (2014).
- Di Antonio, M. et al. Single-molecule visualization of DNA G-quadruplex formation in live cells. *Nat. Chem.* **12**, 832–837 (2020).
- Hänsel-Hertsch, R. et al. G-quadruplex structures mark human regulatory chromatin. *Nat. Genet.* **48**, 1267–1272 (2016).
- Hänsel-Hertsch, R., Spiegel, J., Marsico, G., Tannahill, D. & Balasubramanian, S. Genome-wide mapping of endogenous G-quadruplex DNA structures by chromatin immunoprecipitation and high-throughput sequencing. *Nat. Protoc.* **13**, 551–564 (2018).
- Hänsel-Hertsch, R. et al. Landscape of G-quadruplex DNA structural regions in breast cancer. *Nat. Genet.* **52**, 878–883 (2020).
- Esain-Garcia, I. et al. G-quadruplex DNA structure is a positive regulator of MYC transcription. *Proc. Natl Acad. Sci. USA* **121**, e2320240121 (2024).
- Chen, Y. et al. An upstream G-quadruplex DNA structure can stimulate gene transcription. *ACS Chem. Biol.* **19**, 736–742 (2024).
- Spiegel, J. et al. G-quadruplexes are transcription factor binding hubs in human chromatin. *Genome Biol.* **22**, 117 (2021).
- Lago, S. et al. Promoter G-quadruplexes and transcription factors cooperate to shape the cell type-specific transcriptome. *Nat. Commun.* **12**, 3885 (2021).
- Zhang, X., Spiegel, J., Martínez Cuesta, S., Adhikari, S. & Balasubramanian, S. Chemical profiling of DNA G-quadruplex-interacting proteins in live cells. *Nat. Chem.* **13**, 626–633 (2021).

22. Shen, J. et al. Promoter G-quadruplex folding precedes transcription and is controlled by chromatin. *Genome Biol.* **22**, 143 (2021).
23. Rodriguez, R. et al. Small-molecule-induced DNA damage identifies alternative DNA structures in human genes. *Nat. Chem. Biol.* **8**, 301–310 (2012).
24. Marchetti, C. et al. Targeting multiple effector pathways in pancreatic ductal adenocarcinoma with a G-quadruplex-binding small molecule. *J. Med. Chem.* **61**, 2500–2517 (2018).
25. Wang, X. et al. Conformational switching of G-quadruplex DNA by photoregulation. *Angew. Chem. Int. Ed.* **49**, 5305–5309 (2010).
26. Murat, P., Gormally, M. V., Sanders, D., Di Antonio, M. & Balasubramanian, S. Light-mediated in cell downregulation of G-quadruplex-containing genes using a photo-caged ligand. *Chem. Commun.* **49**, 8453–8455 (2013).
27. O'Hagan, M. P. et al. A photoresponsive stiff-stilbene ligand fuels the reversible unfolding of G-quadruplex DNA. *Angew. Chem. Int. Ed.* **58**, 4334–4338 (2019).
28. O'Hagan, M. P. et al. Visible-light photoswitching of ligand binding mode suggests G-quadruplex DNA as a target for photopharmacology. *Chem. Commun.* **56**, 5186–5189 (2020).
29. Ramos-Soriano, J. & Galan, M. C. Photoresponsive control of G-quadruplex DNA systems. *JACS Au* **1**, 1516–1526 (2021).
30. Lerch, M. M., Hansen, M. J., van Dam, G. M., Szymanski, W. & Feringa, B. L. Emerging targets in photopharmacology. *Angew. Chem. Int. Ed.* **55**, 10978–10999 (2016).
31. Siewertsen, R. et al. Highly efficient reversible Z–E photoisomerization of a bridged azobenzene with visible light through resolved S1(nπ\*) absorption bands. *J. Am. Chem. Soc.* **131**, 15594–15595 (2009).
32. Trads, J. B. et al. Sign inversion in photopharmacology: incorporation of cyclic azobenzenes in photoswitchable potassium channel blockers and openers. *Angew. Chem. Int. Ed.* **58**, 15421–15428 (2019).
33. Cabré, G. et al. Synthetic photoswitchable neurotransmitters based on bridged azobenzenes. *Org. Lett.* **21**, 3780–3784 (2019).
34. Rodriguez, R. et al. A novel small molecule that alters shelterin integrity and triggers a DNA-damage response at telomeres. *J. Am. Chem. Soc.* **130**, 15758–15759 (2008).
35. Hittinger, A. et al. Chemical derivatives binding very specifically with G-quadruplex DNA structures and use thereof as a specific anti-cancer agent. International patent WO 2004072027 (2004).
36. Guilbaud, G. et al. Local epigenetic reprogramming induced by G-quadruplex ligands. *Nat. Chem.* **9**, 1110–1117 (2017).
37. Monchaud, D. & Teulade-Fichou, M. P. A hitchhiker's guide to G-quadruplex ligands. *Org. Biomol. Chem.* **6**, 627–636 (2008).
38. Lipinski, C. A., Lombardo, F., Dominy, B. W. & Feeney, P. J. Experimental and computational approaches to estimate solubility and permeability in drug discovery and development settings. *Adv. Drug Deliv. Rev.* **23**, 3–25 (1997).
39. Monchaud, D., Allain, C. & Teulade-Fichou, M. P. Development of a fluorescent intercalator displacement assay (G4-FID) for establishing quadruplex-DNA affinity and selectivity of putative ligands. *Bioorg. Med. Chem. Lett.* **16**, 4842–4845 (2006).
40. Das, R. N., Andréasson, M., Kumar, R. & Chorell, E. Macrocyclization of bis-indole quinolines for selective stabilization of G-quadruplex DNA structures. *Chem. Sci.* **11**, 10529–10537 (2020).
41. Koirala, D. et al. Long-loop G-quadruplexes are misfolded population minorities with fast transition kinetics in human telomeric sequences. *J. Am. Chem. Soc.* **135**, 2235–2241 (2013).
42. Li, Y., Liu, C., Feng, X., Xu, Y. & Liu, B. F. Ultrafast microfluidic mixer for tracking the early folding kinetics of human telomere G-quadruplex. *Anal. Chem.* **86**, 4333–4339 (2014).
43. Biswas, A. et al. Stabilization and fluorescence light-up of G-quadruplex nucleic acids using indolyl-quinolinium based probes. *Phys. Chem. Chem. Phys.* **24**, 6238–6255 (2022).
44. Müller, S., Kumari, S., Rodriguez, R. & Balasubramanian, S. Small-molecule-mediated G-quadruplex isolation from human cells. *Nat. Chem.* **2**, 1095–1098 (2010).
45. Rodriguez, R. & Miller, K. M. Unravelling the genomic targets of small molecules using high-throughput sequencing. *Nat. Rev. Genet.* **15**, 783–796 (2014).
46. Yu, Z. et al. Chem-map profiles drug binding to chromatin in cells. *Nat. Biotechnol.* **41**, 1265–1271 (2023).
47. Rory, S. & Gord, B. DiffBind: differential binding analysis of ChIP-Seq peak. <http://bioconductor.org/packages/release/bioc/vignettes/DiffBind/inst/doc/DiffBind.pdf> (2011).
48. Chambers, V. S. et al. High-throughput sequencing of DNA G-quadruplex structures in the human genome. *Nat. Biotechnol.* **33**, 877–881 (2015).
49. Hui, W. W. I., Simeone, A., Zyner, K. G., Tannahill, D. & Balasubramanian, S. Single-cell mapping of DNA G-quadruplex structures in human cancer cells. *Sci. Rep.* **11**, 23641 (2021).
50. Balasubramanian, S., Hurley, L. H. & Neidle, S. Targeting G-quadruplexes in gene promoters: a novel anticancer strategy? *Nat. Rev. Drug Discov.* **10**, 261–275 (2011).
51. Herzog, V. A. et al. Thiol-linked alkylation of RNA to assess expression dynamics. *Nat. Methods* **14**, 1198–1204 (2017).
52. Muhar, M. et al. SLAM-seq defines direct gene-regulatory functions of the BRD4-MYC axis. *Science* **805**, 800–805 (2018).
53. Zyner, K. G. et al. G-quadruplex DNA structures in human stem cells and differentiation. *Nat. Commun.* **13**, 142 (2022).

**Publisher's note** Springer Nature remains neutral with regard to jurisdictional claims in published maps and institutional affiliations.

**Open Access** This article is licensed under a Creative Commons Attribution 4.0 International License, which permits use, sharing, adaptation, distribution and reproduction in any medium or format, as long as you give appropriate credit to the original author(s) and the source, provide a link to the Creative Commons licence, and indicate if changes were made. The images or other third party material in this article are included in the article's Creative Commons licence, unless indicated otherwise in a credit line to the material. If material is not included in the article's Creative Commons licence and your intended use is not permitted by statutory regulation or exceeds the permitted use, you will need to obtain permission directly from the copyright holder. To view a copy of this licence, visit <http://creativecommons.org/licenses/by/4.0/>.

© The Author(s) 2025

## Methods

### Chemical synthesis and characterizations

Full synthesis and characterization of molecules, photoisomerization details, UV-visible spectroscopy, cell viability assays, western blotting and general information are described in Supplementary Information. PDS was synthesized as previously reported<sup>34</sup>. Physicochemical properties of the compounds were calculated using ChemAxon MarvinSketch (version 21.4.0, <http://www.chemaxon.com>).

### FID assay

The protocol was adapted from that previously reported<sup>54</sup>. HPLC-purified DNA oligonucleotides (G4 MYC, 5'-TGAGGGTGGGTAGGGTGGGTAA-3'; dsDNA, 5'-CAATCGGATCGAATTCGATCCGATTG-3')<sup>54,55</sup> were purchased from Merck and annealed at 5  $\mu\text{M}$  in the assay buffer (10 mM lithium cacodylate, pH 7.3, 100 mM KCl) at 95 °C for 5 min and slowly cooling to room temperature. A mixture of 2.5  $\mu\text{M}$  annealed oligonucleotides and TO (5  $\mu\text{M}$  for G4 MYC, 7.5  $\mu\text{M}$  for dsDNA) was prepared and added to a 96-well plate (HSP9655, Bio-Rad) at 10  $\mu\text{l}$  per well. Ligand solutions (10  $\mu\text{M}$  or 50  $\mu\text{M}$  in assay buffer) were added along the line, followed by adding assay buffer to make ligand concentration series 0–5  $\mu\text{M}$  or 0–20  $\mu\text{M}$ , with the total volume adjusted to 100  $\mu\text{l}$  per well. The plate was sealed, centrifuged (500  $\times$  g, 1 min) and incubated with orbital shaking (500 rpm, 3 min). End-point fluorescence was measured on a fluorescence plate reader (BMG PHERAstar Plus) using 485 nm/520 nm filters, with gain adjusted at 80% of the fluorescence from a well without ligand. To measure the binding of *trans* isomers, the same plate was illuminated at 405 nm for 2 min, before the incubation and fluorescence measurement. The percentage of displacement was calculated from the fluorescence intensity ( $F$ ) subtracting buffer absorbance, using the following equation: percentage of displacement =  $100 - [(F/F_0) \times 100]$ , where  $F_0$  is the fluorescence from the fluorescent probe bound to DNA without ligand. FID curves were fitted using a one-site specific binding with the Hill slope model in GraphPad Prism 10 (version 10.2.2) to determine  $\text{DC}_{50}$ . Apparent dissociation constants ( $K_d$ ) were calculated using the following equations with  $K_a^{\text{TO}} = 5.01 \times 10^{-6} \text{ M}^{-1}$  for G4 MYC:  $K_a^{\text{ligand}} = (K_a^{\text{TO}} \times [\text{TO}]) / \text{DC}_{50}$ ,  $K_d^{\text{ligand}} = 1/K_a^{\text{ligand}}$  as described previously<sup>40</sup>. Standard deviations (s.d.) were calculated from three or four replicates ( $n = 3$  or 4).

### CD titrations

CD spectra were recorded on an Applied Photophysics Chirascan Plus CD spectrometer using a 1 mm path length quartz cuvette at 20 °C, with the following scanning parameters: 220–330 nm or 220–450 nm, 0.5 s response time, 1 nm intervals and 1 nm bandwidth. For titration experiments, HPLC-purified G4 DNA oligonucleotides (G4 MYC, 5'-TGAGGGTGGGTAGGGTGGGTAA-3'; G4 KIT1, 5'-AGGGAGGGCGTCTGGGAGGAGGG-3')<sup>55,56</sup> were purchased from Merck and annealed in 10 mM Tris-HCl (pH 7.4) with 100 mM LiCl. Indicated amounts of **9** were added to make a final concentration of 10  $\mu\text{M}$  oligonucleotides. After a 2 min equilibration, the same sample was measured before and after 1 min of 405 nm illumination, followed by another measurement after 1 min of 525 nm illumination. Reported spectra, plotted using GraphPad Prism 10 (version 10.2.2), represent a smoothed average of three scans, with baseline correction against the buffer and zero adjustment at 330 nm. Molar ellipticity ( $\theta$ ) is quoted in  $\times 10^5 \text{ deg cm}^2 \text{ dmol}^{-1}$ .

### Cell culture

Human osteosarcoma U2OS cells (ATCC, HTB-96) were cultured in phenol red-free Dulbecco's modified Eagle medium (DMEM) (high glucose and L-glutamine plus, Gibco, catalogue number 21063045) supplemented with 10% (v/v) heat-inactivated fetal bovine serum (Gibco, catalogue number 10082147) and 1 mM sodium pyruvate (hereafter referred to as full-growth DMEM media). Cells were maintained at 37 °C in a humidified 5%  $\text{CO}_2$  atmosphere. After thawing, cells were passaged at least twice before use in experiments. Periodic tests confirmed that the cells were mycoplasma-free.

### G4switch Chem-map

The protocol was adapted from that previously described<sup>46</sup>. U2OS cells were grown to a 70–80% confluence. Cells were detached with Accutase (Gibco, catalogue number A1110501), quenched with full-growth DMEM media and centrifuged (200  $\times$  g, 5 min). Cell pellets were fixed in 0.1% (w/v) formaldehyde in PBS for 2 min at room temperature and then quenched with a final concentration of 110 mM glycine. Cells were centrifuged (300  $\times$  g, 5 min, 4 °C) and resuspended in cold wash buffer (20 mM HEPES, pH 7.5, 150 mM KCl, 0.5 mM spermidine, cOmplete EDTA-free protease inhibitor cocktail (Roche, catalogue number 11836170001)). Cells were either used directly or stored frozen in wash buffer containing 10% (v/v) DMSO at  $-80$  °C until use. A final density of 6 million cells per ml was used.

G4switch-biotin stock solution in DMSO was diluted to 10  $\mu\text{M}$  in antibody buffer (wash buffer containing 2 mM EDTA, 0.1% bovine serum albumin, 0.05% digitonin). The solution was either kept in the dark or illuminated at 405 nm for 2 min to obtain the *cis* and *trans* G4switch-biotin, respectively. For each sample, 4  $\mu\text{l}$  of 10  $\mu\text{M}$  *cis* or *trans* G4switch-biotin and 3.4  $\mu\text{l}$  anti-biotin (D5A7) rabbit mAb (Cell Signaling Technology, catalogue number 55975;  $\sim 10$   $\mu\text{M}$ ) were added to 32.6  $\mu\text{l}$  of antibody buffer to make a final volume of 40  $\mu\text{l}$ . The mixture was incubated in the dark or under pulsed 405 nm illumination (1.5 s every 15 s) inside a light-proof box at 4 °C for 1 h to form a high-concentration precomplex. Next, 60  $\mu\text{l}$  of antibody buffer was added to the precomplex, resulting in a final concentration of 0.4  $\mu\text{M}$  precomplex solution based on the G4switch-biotin concentration, with the anti-biotin antibody diluted to a final ratio of  $\sim 1:30$ .

Concanavalin A beads (15  $\mu\text{l}$ ) (Bangs Laboratories, catalogue number BP531) per sample were washed twice in binding buffer (20 mM HEPES, pH 7.5, 10 mM KCl, 1 mM  $\text{CaCl}_2$ , 1 mM  $\text{MnCl}_2$ ) and resuspended in 10  $\mu\text{l}$  of binding buffer. A 100  $\mu\text{l}$  cell suspension was incubated with 10  $\mu\text{l}$  of prewashed concanavalin A beads in a 0.2 ml colourless transparent PCR tube on an Intelli Mixer RM-2M (ELMI) set to mode C3 at 20 rpm with the following mixing cycle: 6 s at 108°, 6 s at 252° and 12 s pause at 0°, for 10 min at room temperature. Bead-bound cells were gently washed twice with 100  $\mu\text{l}$  of wash buffer using a magnet stand and resuspended in 100  $\mu\text{l}$  of G4switch-biotin-anti-biotin precomplex solution. The *trans*-G4switch-biotin sample was illuminated at 405 nm with cooling by a desk fan, while the *cis* isomer was kept in the dark by wrapping the tube with foil. Samples without precomplex were used as controls. All samples were incubated on the mixer using the same mixing programme at room temperature for 2 h.

Cells were washed three times in 200  $\mu\text{l}$  Dig-wash buffer (wash buffer containing 0.05% digitonin) to remove unbound antibodies. They were then incubated in 100  $\mu\text{l}$  of a 1:100 dilution of guinea pig anti-rabbit IgG secondary antibody (antibodies-online, catalogue number ABIN101961) in Dig-wash buffer on the mixer using the above mixing programme at room temperature for 1 h, with or without 405 nm illumination with cooling by a desk fan for the *trans* and *cis* probe isomers.

pA-Tn5 conjugated with sequencing adapters were prepared as previously described<sup>49</sup>. pA-Tn5 adapter complex (the pA-Tn5 concentration is 2  $\mu\text{M}$ ) is diluted 1:200 into Dig-300 buffer (20 mM HEPES, pH 7.5, 300 mM KCl, 0.5 mM spermidine, 0.01% digitonin, cOmplete EDTA-free protease inhibitor cocktail). Cells were then washed three times in 200  $\mu\text{l}$  Dig-wash buffer to remove unbound antibodies before incubating in 100  $\mu\text{l}$  pA-Tn5 adapter complex solution on the mixer using the above mixing programme at room temperature for 1 h, with or without 405 nm illumination for the *trans* and *cis* probe isomers. Cells were then washed three times with 200  $\mu\text{l}$  Dig-300 buffer to remove unbound pA-Tn5 before incubation in 200  $\mu\text{l}$  tagmentation buffer (Dig-300 buffer containing 10 mM  $\text{MgCl}_2$ ) on the mixer using the above mixing programme at 37 °C for 1 h, in the presence and absence of 405 nm illumination for the *trans* and *cis* probe isomers.

Cells were washed twice in 200  $\mu\text{l}$  TAPS wash buffer (10 mM TAPS, 0.2 mM EDTA) and resuspended in 100  $\mu\text{l}$  extraction buffer (10 mM

Tris-HCl, pH 8.0, 0.5 mg ml<sup>-1</sup> proteinase K (Thermo Scientific, catalogue number E00491), 0.5% SDS) with vortexing. The suspension was incubated at 55 °C for 1.5 h at 800 rpm. DNA extraction was performed using the DNA Clean & Concentrator-5 kit (Zymo Research, catalogue number D4013). DNA was eluted in 25 µl of the provided DNA elution buffer after a 10 min incubation at room temperature.

To amplify DNA libraries, PCR was performed by mixing 21 µl tagged DNA with 2 µl uniquely barcoded v2 Ad1.x primer (10 µM) and 2 µl uniquely barcoded v2 Ad2.x primer (10 µM)<sup>57</sup>, and 25 µl NEBNext Ultra II Q5 2× PCR Master mix (New England Biolabs, catalogue number M0544) using the following cycle: 72 °C for 5 min; 98 °C for 30 s; 10 cycles of 98 °C for 10 s and 63 °C for 10 s; 72 °C for 1 min. Libraries were cleaned up by adding 1.3× volume (65 µl) of Ampure XP beads (Beckman Coulter, catalogue number A63882), incubated at room temperature for 10 min and washed gently twice with 200 µl of 80% ethanol. DNA was eluted in 25 µl of 10 mM Tris-HCl, pH 8.0.

The size distribution of libraries was confirmed by TapeStation analysis using High Sensitivity D1000 ScreenTape (Agilent, catalogue number 5067-5584). Libraries were quantified using the NEBNext Library Quant Kit (New England Biolabs, catalogue number E7630L). Libraries were balanced and pooled, followed by size selection by adding 0.4× volume of Ampure XP beads and incubation at room temperature for 10 min. The supernatant was transferred to a new DNA LoBind tube, and 1.3× volume of Ampure XP beads was then added and incubated at room temperature for 10 min. On-bead libraries were washed twice with 80% ethanol and eluted in 30 µl of 10 mM Tris-HCl, pH 8.0. Paired-end sequencing of libraries was performed on a NextSeq 2000 sequencer (Illumina) using the NextSeq 1000/2000 P2 reagent kit (100 cycles) (Illumina, catalogue number 20046811). Experiments were performed in three independent biological replicates, each with three technical replicates.

For the Chem-map competition experiments, U2OS cells were grown to a 70–80% confluence and treated with PDS (4 µM or 20 µM) or vehicle DMSO at 37 °C for 3 h. Cells were then washed twice with PBS and processed according to the standard G4switch Chem-map protocol. Three independent biological replicates were conducted.

#### G4-CUT&Tag

The G4-CUT&Tag was adapted from that previously described<sup>49</sup>, and performed in five replicates. The BG4 (scFv) antibody was expressed as previously reported<sup>11,15</sup>. pA-Tn5 adapter complex was prepared as described previously<sup>49</sup>. Concanavalin A-coated beads were prepared with Dynabeads MyOne Streptavidin T1 beads (Invitrogen, catalogue number 65601) and biotin-conjugated concanavalin A solution (Sigma-Aldrich, catalogue number C2272) as described previously<sup>58</sup>. In brief, U2OS cells (~300,000 cells per 100 µl for each sample) were bound to concanavalin A-conjugated beads (10 µl). The bead-bound cells were permeabilized and incubated in 50 µl of ~600 nM BG4 antibody solution diluted in antibody buffer at 4 °C overnight, followed by an incubation in 50 µl rabbit anti-FLAG antibody (Cell Signaling Technology, catalogue number 2368S) solution at a 1:25 dilution in Dig-wash buffer at room temperature for 1 h. After a further incubation with 50 µl guinea pig anti-rabbit IgG secondary antibody solution at a 1:100 dilution in Dig-wash buffer at room temperature for 1 h, 50 µl pA-Tn5 adapter complex dilution at a 1:250 dilution in Dig-300 buffer was added to cells for incubation at room temperature for 1 h, followed by the tagmentation reaction at 37 °C for 1 h. After proteinase K digestion, the DNA fragments were extracted for the library preparation and Illumina sequencing.

#### SLAM-seq

About 2.1 × 10<sup>5</sup> U2OS cells per well were seeded in a 6-well plate in full-growth DMEM media and grown for 24 h. In one set of experiments, U2OS cells were treated with **9** (6 µM) in 1 ml full-growth DMEM media at 37 °C for 30 min, in the presence and absence of pulsed 405 nm light illumination (90 s of continuous 405 nm illumination for maximum

*cis*-to-*trans* photoisomerization, followed by light pulses of 75 ms every 15 s to maintain activation of **9** with minimal light exposure), to determine the effects of *cis* and *trans* isomers, respectively. In a 'rescue' experiment, alternating pulses of 405 nm and 525 nm light illumination, which involves 90 s of 405 nm illumination, 120 s of 525 nm illumination, and pulses of alternating phases of 75 ms 405 nm and 375 ms 525 nm every 15 s, to measure the effects of cycles of reversibly photoswitching **9** on and off, ending with the off state. **9** with only pulsed 525 nm light illumination (120 s of continuous 525 nm illumination followed by pulses of 375 ms every 15 s) served as a control. All conditions were compared with a non-illuminated DMSO control. After the 30 min treatment under all conditions, newly synthesized RNA was then labelled by incubating the cells with 250 µM 4sU (Sigma-Aldrich, catalogue number T4509) at 37 °C for 60 min in the dark. Cells were washed twice with 2 ml PBS, followed by RNA extraction using the RNeasy Plus Mini Kit (QIAGEN, catalogue number 74134). Total RNA was quantified by a Nanodrop One (Thermo Fisher Scientific), and 3 µg of RNA was subjected to iodoacetamide alkylation using the SLAMseq Kinetics Kit (Lexogen, catalogue number O61). Alkylated RNA (500 ng) was then used for preparation of 3'-end mRNA sequencing libraries using the QuantSeq 3' mRNA-Seq Library Prep kit (FWD) (Lexogen, catalogue number O15) and PCR Add-on kit (Lexogen, catalogue number O20) for Illumina. Libraries were sequenced on a NextSeq 500 sequencer (Illumina) using the High Output kit (Illumina, catalogue number FC-404-2005). Four independent biological replicates were performed ( $n = 4$ ).

#### Crystal violet staining and cell density quantification

The protocol was adapted from that previously described<sup>59</sup>. In brief, U2OS cells were seeded at a density of 35,000 cells per well in full-growth DMEM media in a 6-well plate and grown for 24 h. Cells were then cultured in the presence of 125 nM **9** compared with vehicle DMSO in 1.5 ml full-growth DMEM media, with half of the wells shielded from the pulsed 405 nm illumination (60 s continuous illumination followed by pulses of 75 ms every 22.5 s) for 72 h. Cells were washed with 2 ml PBS, stained with 1 ml crystal violet solution (0.5% crystal violet in 20% methanol) at room temperature for 10 min. Unbound crystal violet was removed by rinsing in distilled water (2 ml 4×) and cells were subsequently air-dried. Cells were visualized on a Bio-Rad ChemiDoc MP system using the Coomassie Blue Gel channel (S90/110, white trans) with 0.5 s manual exposure. Image processing and cell density quantification were performed using the open-source software Fiji (version 2.14.0/1.54f)<sup>60</sup> (Supplementary Information). Three independent biological replicates were performed ( $n = 3$ ).

#### Chem-map and G4-CUT&Tag analysis

Illumina sequencing paired-end output files (Supplementary Tables 1–3) were demultiplexed using demuxIllumina (version 3.0.9) using the following flags: -c -d -i -e -t -l -r 0.01 -R -l 9. The resulting fastq.gz files underwent sequencing quality control using FastQC (version 0.11.8), and their summary was visualized by MultiQC (version 1.11). Bases with a quality score below 20 were trimmed from both reads using cutadapt (cutadapt -q 20). Fastq files were aligned to the combined hg38 and *Escherichia coli* genomes using bwa (version 0.7.17-r1188) with only reads in the whitelist regions of hg38 continuing the process pipeline. Duplicates were removed using Picard (version 2.20.3) (Picard MarkDuplicates). Peaks were called using Seacr (version 1.3) without input control reporting the top 1% by AUC regions, stringent criteria (Supplementary Tables 4 and 5). BigWig files were created of the bam files, normalized at cpm using deepTools (version 2.0)<sup>61</sup>. Consensus peaks are defined by the overlap of the technical replicates for each biological and two out of three biological replicates for each feature. High-confidence peak regions, unless otherwise stated, are considered those regions at the top 1% by AUC, with minimum total signal 5 (min5) and present in 2 of 3 replicates (multi2). Differential analysis on the

union of all the peaks among the examined molecules was carried out using DiffBind (version 3.10.1)<sup>47,62</sup>.

### SLAM-seq analysis

Illumina sequencing single-end output files (Supplementary Table 6) were demultiplexed using demuxillumina with the following flags: -c -d -i -e -t1 -r 0.01 -l9. The quality of the resulting FASTQ files was assessed using FastQC (version 0.11.8), and bases with a quality score below 20 were trimmed from the read using cutadapt (cutadapt -q 20), with adapter overlaps set to 3 bp for trimming.

Gene and 3' untranslated region annotations were obtained from the UCSC table browser (<https://genome.ucsc.edu/cgi-bin/hgTables>), with Gencode v37 used for transcript annotation.

The SlamDunk package (v.0.3.4) was used to process the trimmed reads to analyse 4sU incorporation events. The full analysis was performed using the 'Slamdunk all' command with the following parameters: -t 5 -s 12 -n 100 -m -mv 0.2 -c 2 -rl 100, aligning against the human genome (GRCh38) and filtering for variants with a variant fraction of 0.2. Reads were filtered for having  $\geq 2$  T > C conversions, unless otherwise stated.

Differential gene expression of TcReadCounts was restricted to genes with  $\geq 10$  reads in at least one condition. DESeq2 (version 1.2.10) was used for differential gene expression analysis on raw read counts with  $\geq 2$  T > C conversions using default settings. Size factors were calculated based on corresponding total read counts for global normalization. Volcano plots were generated using the EnhancedVolcano package (v.1.16.0). Plots of differential gene expression were visualized using the ggplot2 package in R (version 4.1) with significant genes ( $q \leq 0.05$ ,  $|\log_2FC| \geq 1$ ).

### Reporting summary

Further information on research design is available in the Nature Portfolio Reporting Summary linked to this article.

### Data availability

Sequencing data reported in this study have been deposited in the NCBI Gene Expression Omnibus (GEO) repository under accession number [GSE261837](https://www.ncbi.nlm.nih.gov/geo/query/acc.cgi?acc=GSE261837). The previously published GRCh38 (hg38) ([https://www.ensembl.org/Homo\\_sapiens/Info/Index](https://www.ensembl.org/Homo_sapiens/Info/Index)) and OQs ([GSE110582](https://www.ncbi.nlm.nih.gov/geo/query/acc.cgi?acc=GSE110582))<sup>48</sup> datasets were used. Source data are provided with this paper.

### Code availability

All detailed bioinformatics scripts are available at <https://github.com/sblab-informatics/G4-switch>.

### References

- Largy, E., Hamon, F. & Teulade-Fichou, M. P. Development of a high-throughput G4-FID assay for screening and evaluation of small molecules binding quadruplex nucleic acid structures. *Anal. Bioanal. Chem.* **400**, 3419–3427 (2011).
- Ambrus, A., Chen, D., Dai, J., Jones, R. A. & Yang, D. Solution structure of the biologically relevant G-quadruplex element in the human c-MYC promoter. Implications for G-quadruplex stabilization. *Biochemistry* **44**, 2048–2058 (2005).
- Phan, A. T., Kuryavyy, V., Burge, S., Neidle, S. & Patel, D. J. Structure of an unprecedented G-quadruplex scaffold in the human c-kit promoter. *J. Am. Chem. Soc.* **129**, 4386–4392 (2007).
- Buenrostro, J. D. et al. Single-cell chromatin accessibility reveals principles of regulatory variation. *Nature* **523**, 486–490 (2015).
- Fujiwara, Y. et al. Preparation of optimized concanavalin A-conjugated Dynabeads® magnetic beads for CUT&Tag. *PLoS ONE* **16**, e0259846 (2021).
- Saotome, K., Morita, H. & Umeda, M. Cytotoxicity test with simplified crystal violet staining method using microtitre plates and its application to injection drugs. *Toxicol. In Vitro* **3**, 317–321 (1989).

- Schindelin, J. et al. Fiji: an open-source platform for biological-image analysis. *Nat. Methods* **9**, 676–682 (2012).
- Ramírez, F. et al. deepTools2: a next generation web server for deep-sequencing data analysis. *Nucleic Acids Res.* **44**, W160–W165 (2016).
- Ross-Innes, C. S. et al. Differential oestrogen receptor binding is associated with clinical outcome in breast cancer. *Nature* **481**, 389–393 (2012).

### Acknowledgements

We thank A. Bruckbauer at the Light Microscopy Core Facility and the staff at the Genomics Core Facility at Cancer Research UK Cambridge Institute for assistance in image quantification analysis and acquiring sequencing data, respectively. We thank D. Howe and P. Gierth at the NMR facility at Yusuf Hamied Department of Chemistry, University of Cambridge, for assistance in acquiring NMR data. We thank M. Farrow at Yusuf Hamied Department of Chemistry, University of Cambridge, for proofreading the paper. We thank M. Di Antonio for the helpful discussion on this study and S. Galli for the assistance in imaging experiments. The Balasubramanian laboratory is financially supported by Cancer Research UK core (SEBINT-2024/100003) and programme award funding (C9681/A29214) and Herchel Smith Funds. S.B. is an investigator of the Wellcome Trust (209441/Z/17/Z).

### Author contributions

X.Z. and S.B. conceived this study. X.Z. led the project and performed the design, synthesis and biophysical characterization of the G4switch and G4switch-biotin. X.Z. and Y.C. conducted the SLAM-seq experiments, and S.D. and A.S. performed the bioinformatic analysis of the SLAM-seq data. X.Z. and Z.Y. performed the G4switch Chem-map and G4-CUT&Tag experiments, and X.Z. performed the Chem-map competition experiments. L.M. performed the bioinformatic analysis of the Chem-map and G4-CUT&Tag data. X.Z. performed the crystal violet staining experiments and cell density quantification with the support of J.S., as well as western blot experiments, and calculated the theoretical physiochemical properties of compounds with the support of S.A. All the authors interpreted the results. X.Z. and S.B. wrote the paper, with contributions from all authors.

### Competing interests

S.B. is a founder and shareholder of biomodal, GenomeTx, Elyx and RNAvate. L.M. is a paid consultant for GenomeTx. A.S. is an employee of QIAGEN. J.S. is an employee of GenomeTx. S.A. is an employee of BenevolentAI. The other authors declare no competing interests.

### Additional information

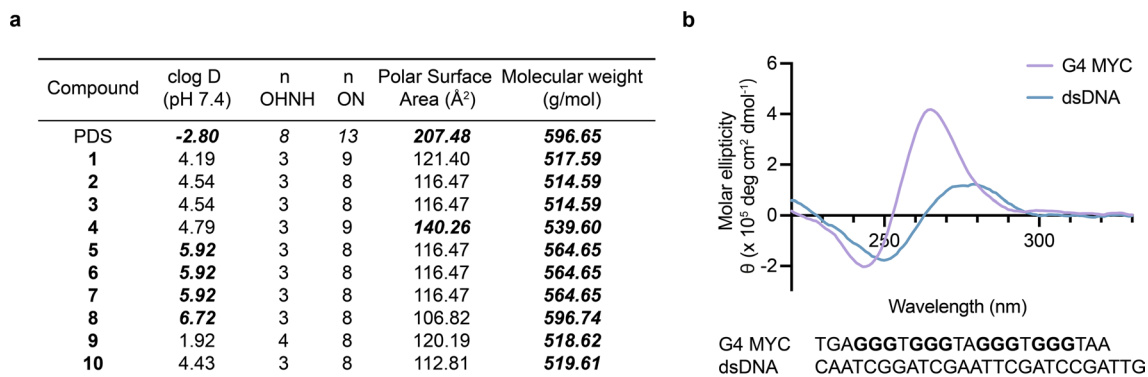
**Extended data** is available for this paper at <https://doi.org/10.1038/s41557-025-01792-1>.

**Supplementary information** The online version contains supplementary material available at <https://doi.org/10.1038/s41557-025-01792-1>.

**Correspondence and requests for materials** should be addressed to Shankar Balasubramanian.

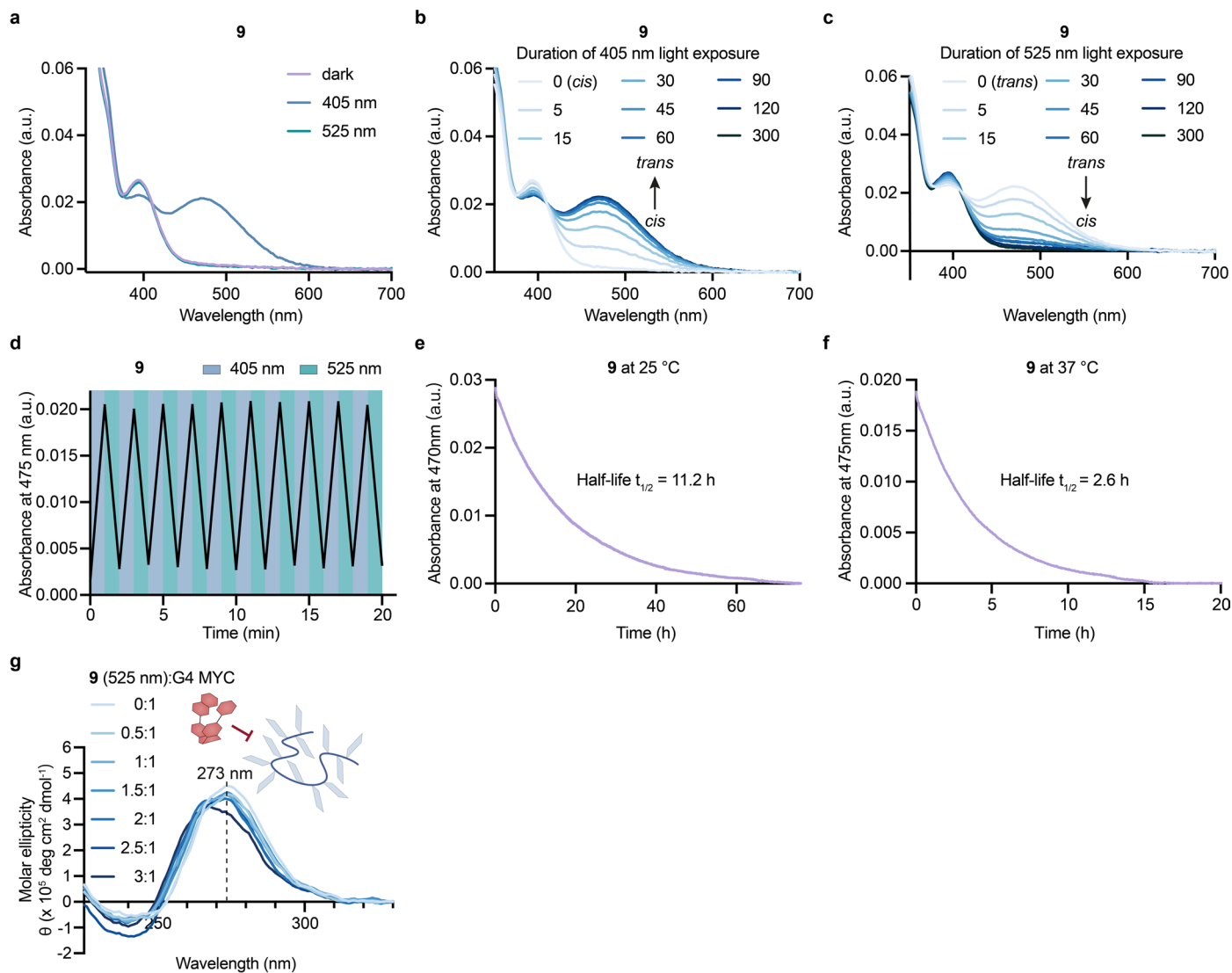
**Peer review information** *Nature Chemistry* thanks Sara Richter and Raphaël Rodriguez for their contribution to the peer review of this work.

**Reprints and permissions information** is available at [www.nature.com/reprints](http://www.nature.com/reprints).



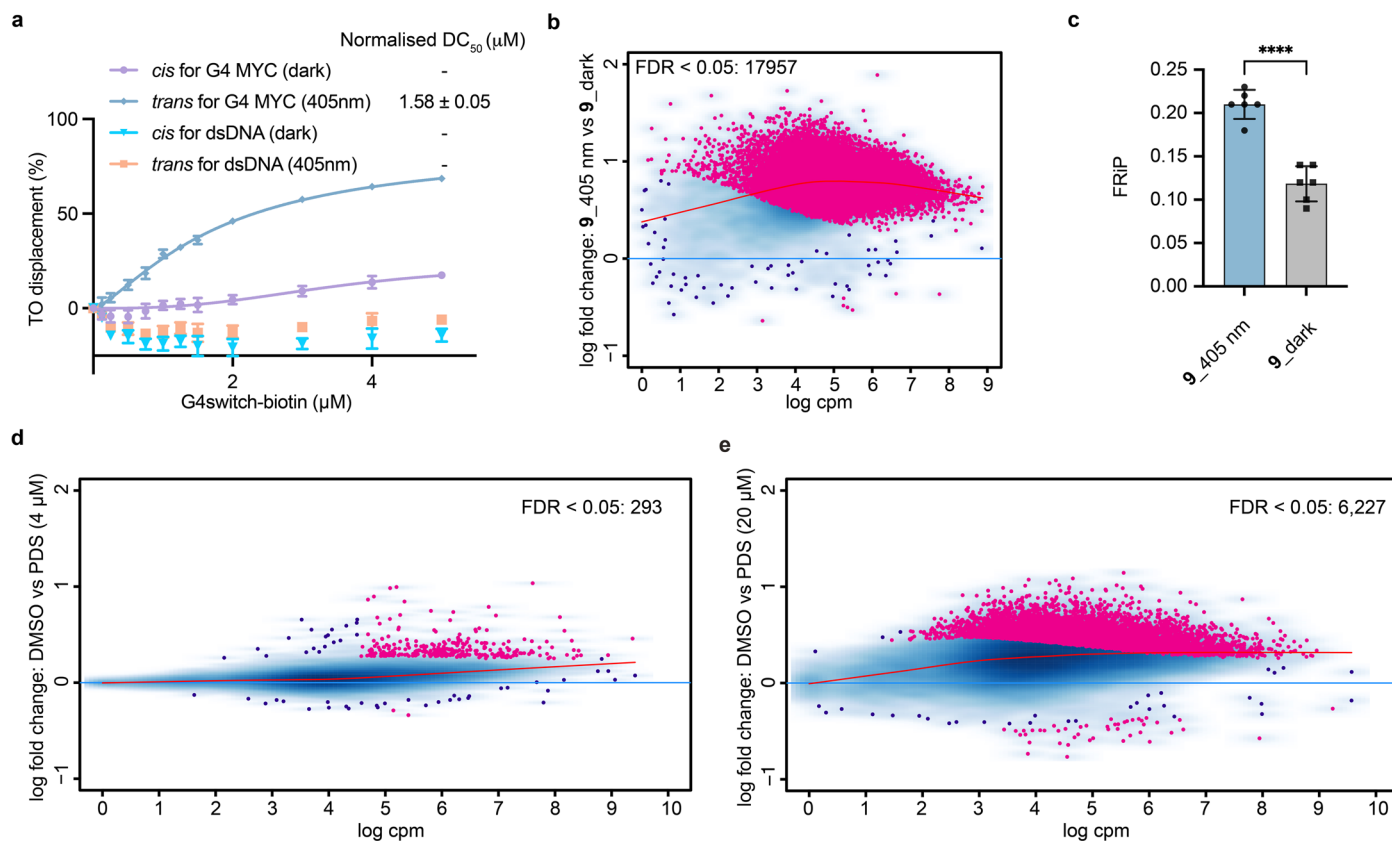
**Extended Data Fig. 1 | Assessment of the putative G4switches.** **a**, Calculated physicochemical properties of PDS and the putative G4switches. Values highlighted in bold italics indicate violation of Lipinski's rule of five: clog D, partition coefficient ( $\leq 5$ ); n OHNH, number of hydrogen bond donors ( $\leq 5$ );

n ON, number of hydrogen bond acceptors ( $\leq 10$ ); Polar surface area ( $80 - 140 \text{ \AA}^2$ ); Molecular weight ( $\leq 500 \text{ Da}$ ). **b**, Structure verification of  $5 \mu\text{M}$  G4 MYC (G-runs are highlighted in bold) and dsDNA control used in the FID assay by CD. Mean of three scans ( $n = 3$ ) is shown.



**Extended Data Fig. 2 | Photophysical characterization of **9** and its interactions with G4 DNA.** **a–c**, UV-Vis absorption spectra of 50  $\mu\text{M}$  **9** in PBS, measured **(a)** in the dark, after 405 nm illumination for 2 min and subsequent 525 nm illumination for 2 min, and **(b,c)** after a series of 405 nm and 525 nm illumination durations (0–300 s), starting from the steady dark-adapted state and 405 nm illuminated state, respectively. **d**, UV-Vis absorbance of 50  $\mu\text{M}$  **9** at 475 nm in PBS, measured during consecutive *cis-trans* photoisomerization cycles, alternating between

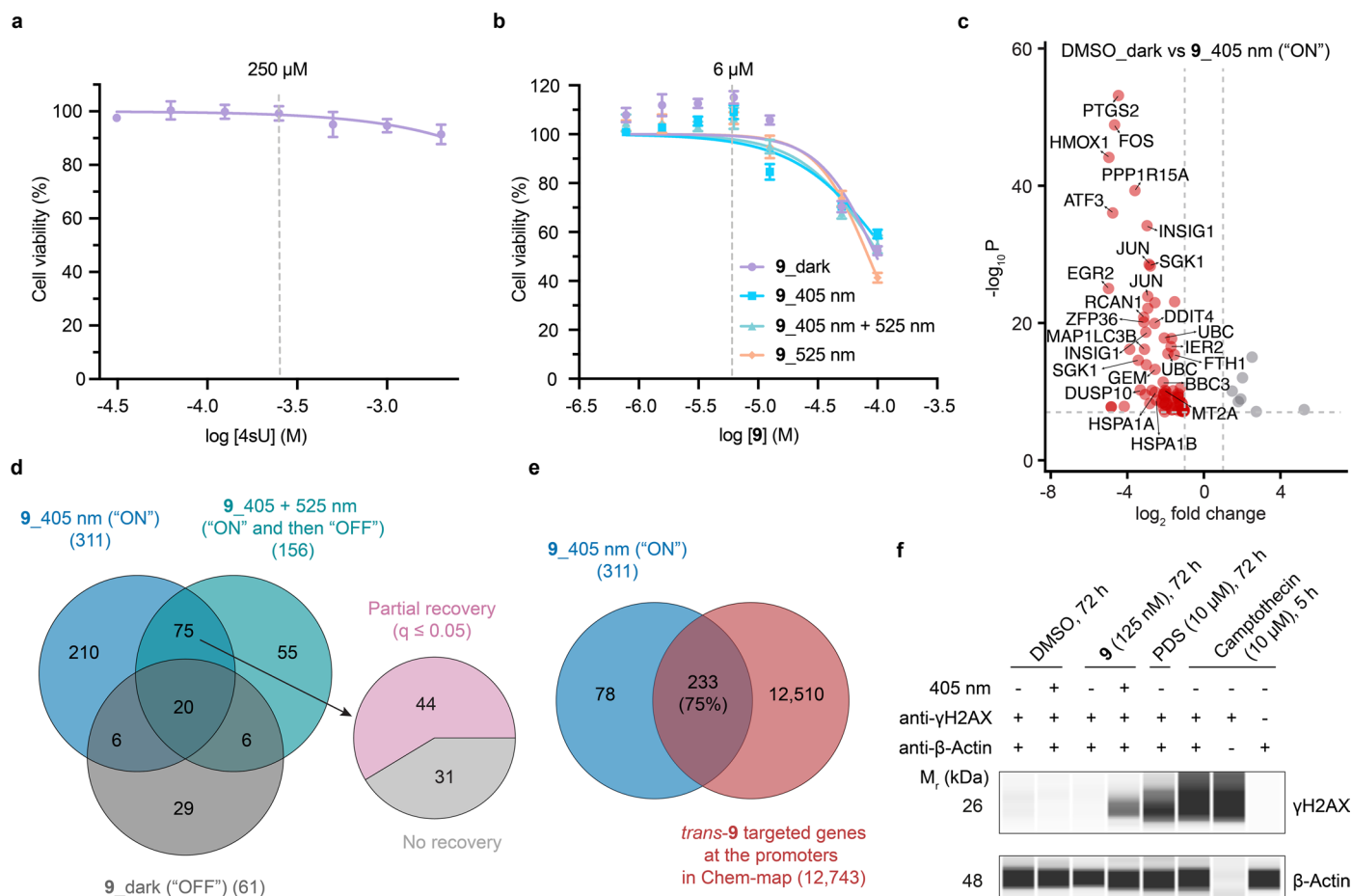
405 nm and 525 nm illuminations. **e,f**, Thermal *trans-to-cis* relaxation of 50  $\mu\text{M}$  **9** in PBS, with half-lives of **(e)**  $t_{1/2} = 11.2$  h at 25 °C and **(f)**  $t_{1/2} = 2.6$  h at 37 °C, measured by recording UV-Vis absorbance of *trans-9* at 470 nm and 475 nm, respectively. **g**, CD spectra of G4 MYC recorded by a titration with increasing amounts of **9** in 10 mM Tris-HCl buffer, 100 mM LiCl, pH 7.4 after further 525 nm illumination for 60 s of the 405 nm illuminated samples shown in Fig. 3e.



### Extended Data Fig. 3 | Genome-wide mapping of binding sites of **9** in cells

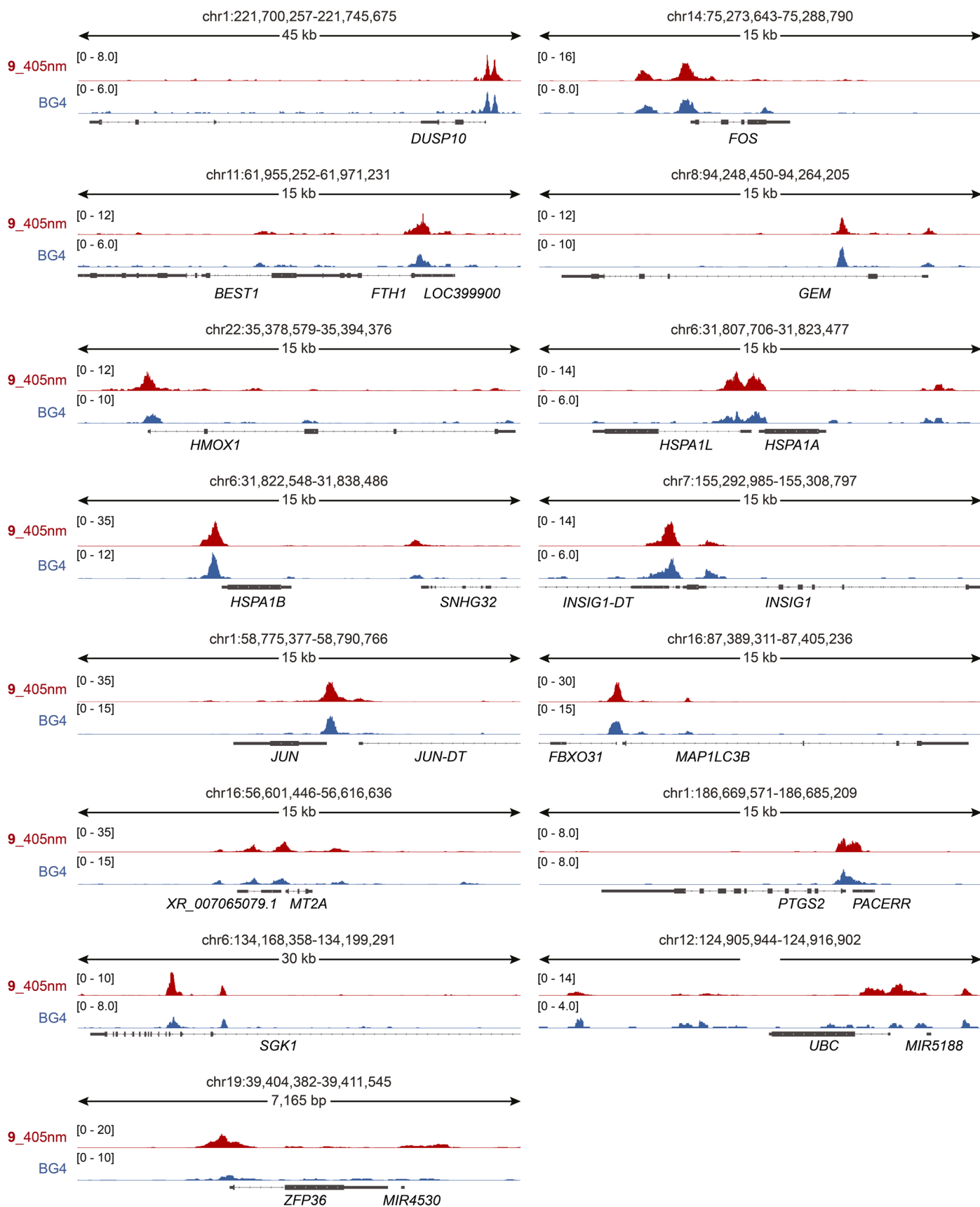
**under light illumination.** **a**, FID curves for G4 MYC and dsDNA induced by increasing concentrations of non-illuminated and 405 nm illuminated G4switch-biotin. The apparent  $K_d$  of *trans*-G4switch-biotin for G4 MYC is  $0.63 \pm 0.02 \mu\text{M}$ , derived from its normalised  $DC_{50}$  ( $1.58 \pm 0.05 \mu\text{M}$ ) (See Methods), while  $K_d$  values for other conditions were not determined within the molecule concentration range (0–5  $\mu\text{M}$ ). Results are shown as mean  $\pm$  s.d. from four replicates ( $n = 4$ ). **b**, Differential binding analysis of the union of Chem-map binding sites across all replicates (three biological replicates, each with three technical replicates) for both isomers of **9** shows 17,957 significantly differentially binding sites of *trans*-**9** compared to the *cis* isomer. Dots highlighted in red represent binding sites that are significantly different (FDR < 0.05) between the two isomers. Positive fold

changes indicate an increase in *trans*-**9** binding. **c**, FRiP analysis comparing the Chem-map profiles of **9** between the 405 nm illuminated *trans* form and non-illuminated *cis* form in U2OS cells. Results represent the mean  $\pm$  s.d. from three biological replicates, each with two technical replicates ( $n = 6$ ). \*\*\*\* $P < 0.0001$ , two-tailed unpaired *t*-test. **d,e**, Differential binding analysis displaying changes in 405 nm illuminated **9** Chem-map binding events across the union of all three biological replicates for pre-treatment with (**d**) 4  $\mu\text{M}$  and (**e**) 20  $\mu\text{M}$  PDS, compared to the vehicle DMSO for 3 h in U2OS cells. Dots highlighted in red represent significantly changing sites (FDR < 0.05) between DMSO and PDS treatments. A positive fold change indicates a decrease in 405 nm illuminated *trans*-**9** binding.

**Extended Data Fig. 4 | G4switch-mediated optical control of gene expression in U2OS cells.**

**a**, Cell viability measured by the Cell Titer-Glo luminescent cell viability assay after treatment of U2OS cells with a series of concentrations of 4sU for 60 min. Results represent the mean  $\pm$  s.d. from four technical replicates ( $n = 4$ ). **b**, Cell viability after treatment with **9** in the dark and under all illumination conditions used in this study for 30 min, followed by 60 min of 4sU (250  $\mu\text{M}$ ) labelling. Results are shown as mean  $\pm$  s.d. from four technical replicates ( $n = 4$ ). **c**, Volcano plot displaying the most significantly downregulated genes (fold change  $>2$ ,  $q < 0.05$ ,  $p < 10^{-8}$ ), highlighted in red, by *trans-9* under pulsed 405 nm illumination compared to the dark-adapted DMSO control. **d**, Venn diagram displaying the overlap of downregulated genes ( $q \leq 0.05$ ) by **9** between dark treatment and 405 nm illumination, and the 405 + 525 nm illumination, compared to the DMSO treatment in the dark. The pie chart illustrates that, among the 75 overlapping downregulated genes

under the 405 nm and 405 + 525 nm illumination conditions, 44 genes show partial recovery (reduced downregulation,  $q \leq 0.05$ ) under the 405 + 525 nm illumination (Supplementary Fig. 6b and Supplementary Table 7), while 31 genes show no recovery compared to the 405 nm condition. **e**, The overlap between downregulated genes (fold change  $>2$ ,  $q < 0.05$ ) by *trans-9* under 405 nm illumination and genes displaying *trans-9* Chem-map binding sites in their promoter regions. **f**, DNA damage marker  $\gamma\text{H2AX}$  was examined by Western blot after treating cells with compound **9** (125 nM) with or without 405 nm illumination (60 s continuous illumination, followed by 75 ms pulses every 22.5 s) and its parent molecule PDS (10  $\mu\text{M}$ ) for 72 h, compared to the dark-adapted DMSO control. Cells treated with Camptothecin, a DNA topoisomerase I inhibitor, for 5 h served as a positive control. A representative image from one of three independent biological replicates with similar results is shown.



**Extended Data Fig. 5 | G4 binding of *trans*-9 in the promoters of several of its most significantly downregulated genes.** Genome browser views display *trans*-9 Chem-map binding sites (red), overlapping with naturally occurring G4

sites mapped by G4-CUT&Tag (blue), at the promoter regions of several genes that are most significantly downregulated by *trans*-9 (fold change >2,  $q \leq 0.05$ ,  $p < 10^{-8}$ ), as randomly selected from those highlighted in Extended Data Fig. 4c.

## Reporting Summary

Nature Portfolio wishes to improve the reproducibility of the work that we publish. This form provides structure for consistency and transparency in reporting. For further information on Nature Portfolio policies, see our [Editorial Policies](#) and the [Editorial Policy Checklist](#).

### Statistics

For all statistical analyses, confirm that the following items are present in the figure legend, table legend, main text, or Methods section.

- | n/a                                 | Confirmed  |
|-------------------------------------|--|
| <input type="checkbox"/>            | <input checked="" type="checkbox"/> The exact sample size ( $n$ ) for each experimental group/condition, given as a discrete number and unit of measurement  |
| <input type="checkbox"/>            | <input checked="" type="checkbox"/> A statement on whether measurements were taken from distinct samples or whether the same sample was measured repeatedly  |
| <input type="checkbox"/>            | <input checked="" type="checkbox"/> The statistical test(s) used AND whether they are one- or two-sided<br><i>Only common tests should be described solely by name; describe more complex techniques in the Methods section.</i>   |
| <input checked="" type="checkbox"/> | <input type="checkbox"/> A description of all covariates tested  |
| <input checked="" type="checkbox"/> | <input type="checkbox"/> A description of any assumptions or corrections, such as tests of normality and adjustment for multiple comparisons   |
| <input type="checkbox"/>            | <input checked="" type="checkbox"/> A full description of the statistical parameters including central tendency (e.g. means) or other basic estimates (e.g. regression coefficient) AND variation (e.g. standard deviation) or associated estimates of uncertainty (e.g. confidence intervals) |
| <input type="checkbox"/>            | <input checked="" type="checkbox"/> For null hypothesis testing, the test statistic (e.g. $F$ , $t$ , $r$ ) with confidence intervals, effect sizes, degrees of freedom and $P$ value noted<br><i>Give <math>P</math> values as exact values whenever suitable.</i>                            |
| <input checked="" type="checkbox"/> | <input type="checkbox"/> For Bayesian analysis, information on the choice of priors and Markov chain Monte Carlo settings  |
| <input checked="" type="checkbox"/> | <input type="checkbox"/> For hierarchical and complex designs, identification of the appropriate level for tests and full reporting of outcomes  |
| <input checked="" type="checkbox"/> | <input type="checkbox"/> Estimates of effect sizes (e.g. Cohen's $d$ , Pearson's $r$ ), indicating how they were calculated  |

*Our web collection on [statistics for biologists](#) contains articles on many of the points above.*

### Software and code

Policy information about [availability of computer code](#)

**Data collection**

NMR data were collected on a Bruker 400 MHz Avance III HD Spectrometer, a 500 MHz Avance III Smart Probe Spectrometer and a 700 MHz TXO Cryoprobe Spectrometer.  
 HRMS data were collected on a Waters LCT Premier (ESI) spectrometer.  
 UV-Vis and CD spectra were collected on a Agilent Cary 3500 UV-Vis spectrophotometer and a Applied Photophysics Chirascan Plus Spectrometer, respectively.  
 FID binding data were collected from a BMG PHERAstar Plus reader.  
 The cell staining images were collected on a Bio-Rad ChemiDoc MP system.  
 A Bio-Rad CFX96 Touch Real-Time PCR Detection System was used for concentration quantification of sequencing libraries.  
 Sequencing data were collected on a NextSeq 500 sequencer (Illumina) and a NextSeq 2000 sequencer (Illumina).

**Data analysis**

Physicochemical properties of compounds were calculated in ChemAxon MarvinSketch (version 21.4.0, <http://www.chemaxon.com>).  
 NMR data were processed in MestReNova (version 12.0.1).  
 UV-Vis, CD titration, and FID assay data were processed and analysed in GraphPad Prism 10 (version 10.2.2).  
 Cell staining images were processed in software Fiji (version 2.14.0/1.54f).  
 Bioinformatics data analyses and processing were performed using Bash, R (version 4.1) and Python (version  $\geq 3.4$ ) programming languages.  
 The following tools were also used: demuxillumina (version 3.0.9), FastQC (version 0.11.8), MultiQC (version 1.11), cutadapt (version 1.18), BWA (version 0.7.17-r1188), Picard (version 2.20.3), Seacr (version 1.3), EnhancedVolcano (v.1.16.0), deepTools (version 2.0), DiffBind (version 3.10.1), Gencode v37, SlamDunk package (v.0.3.4) and DESeq2 (version 1.2.10).  
 The analysis scripts are available on the GitHub page dedicated to this study: <https://github.com/sblab-informatics/G4-switch>

For manuscripts utilizing custom algorithms or software that are central to the research but not yet described in published literature, software must be made available to editors and reviewers. We strongly encourage code deposition in a community repository (e.g. GitHub). See the Nature Portfolio [guidelines for submitting code & software](#) for further information.

## Data

Policy information about [availability of data](#)

All manuscripts must include a [data availability statement](#). This statement should provide the following information, where applicable:

- Accession codes, unique identifiers, or web links for publicly available datasets
- A description of any restrictions on data availability
- For clinical datasets or third party data, please ensure that the statement adheres to our [policy](#)

The sequencing data generated in this study are available at the Gene Expression Omnibus (GEO) repository under accession number GSE261837. The previously published GRCh38 (hg38) ([https://www.ensembl.org/Homo\\_sapiens/Info/Index](https://www.ensembl.org/Homo_sapiens/Info/Index)) and OQs (GSE110582) datasets were used.

## Research involving human participants, their data, or biological material

Policy information about studies with [human participants or human data](#). See also policy information about [sex, gender \(identity/presentation\), and sexual orientation](#) and [race, ethnicity and racism](#).

Reporting on sex and gender

Reporting on race, ethnicity, or other socially relevant groupings

Population characteristics

Recruitment

Ethics oversight

Note that full information on the approval of the study protocol must also be provided in the manuscript.

## Field-specific reporting

Please select the one below that is the best fit for your research. If you are not sure, read the appropriate sections before making your selection.

Life sciences  Behavioural & social sciences  Ecological, evolutionary & environmental sciences

For a reference copy of the document with all sections, see [nature.com/documents/nr-reporting-summary-flat.pdf](https://www.nature.com/documents/nr-reporting-summary-flat.pdf)

## Life sciences study design

All studies must disclose on these points even when the disclosure is negative.

**Sample size** According to a previous Chem-map study (Yu, Z. et al. Nat. Biotechnol. 41, 1265–1271 (2023)), 600,000 cells per sample were used for mapping G4 ligand binding sites; the same number was used in this study. For G4-CUT&Tag, a previous study (Hui, W. I. et al. Sci. Rep. 11, 1–7 (2021)) showed that the total number of G4 peaks mapped increased with cell input, ranging from 10,000 to 100,000 cells. To ensure comprehensive G4 peak capture and minimize underrepresentation, we increased the input to 300,000 cells per sample. For SLAM-seq, 210,000 cells per well were seeded in 6-well plates and grown to 70–80% confluence to ensure sufficient total RNA for iodoacetamide (IAA) alkylation (Lexogen, cat. no. 061) and preparation of 3'-end mRNA sequencing libraries (Lexogen, cat. no. 015) following the manufacturer's protocol (<https://www.lexogen.com/>). For crystal violet staining experiments, 35,000 cells per well in 6-well plates were seeded to ensure appropriate confluence for quantification. For Western blot experiments, 50,000 cells per well were seeded in 6-well plates to ensure adequate protein extraction for analysis using the Jess automated Western blot system (ProteinSimple) following the manufacturer's protocol (<https://www.bio-technie.com/instruments/simple-western>).

**Data exclusions** No data were excluded from analyses in this study.

**Replication** Chem-map experiments were performed in three independent biological replicates, each with three technical replicates, while Chem-map competition experiments were conducted in three independent biological replicates. G4-CUT&Tag was performed in five technical replicates. SLAM-seq was carried out in four biological replicates. Crystal violet staining experiments were conducted in three independent biological replicates (n = 3), with relative cell viability quantified and shown as mean ± standard deviation (s.d.). For Western blot experiments, similar results were obtained in three independent biological replicates. Cell viability assays were performed and are presented as mean ± s.d. from four replicates (n = 4). The FID assay results are shown as mean ± s.d., calculated from three or four technical replicates (n = 3 or 4), while CD spectra were recorded from three scans and presented as the average of the three scans. Similar results were consistently observed in at least two biological replicates for the FID assay and CD experiments. All experiments were reliably reproducible.

**Randomization** No randomization was performed, as control conditions were run in parallel to avoid systematic measurement bias.

## Reporting for specific materials, systems and methods

We require information from authors about some types of materials, experimental systems and methods used in many studies. Here, indicate whether each material, system or method listed is relevant to your study. If you are not sure if a list item applies to your research, read the appropriate section before selecting a response.

### Materials & experimental systems

- |                                     |   |
|-------------------------------------|---|
| n/a                                 | Involved in the study                                     |
| <input type="checkbox"/>            | <input checked="" type="checkbox"/> Antibodies            |
| <input type="checkbox"/>            | <input checked="" type="checkbox"/> Eukaryotic cell lines |
| <input checked="" type="checkbox"/> | <input type="checkbox"/> Palaeontology and archaeology    |
| <input checked="" type="checkbox"/> | <input type="checkbox"/> Animals and other organisms      |
| <input checked="" type="checkbox"/> | <input type="checkbox"/> Clinical data                    |
| <input checked="" type="checkbox"/> | <input type="checkbox"/> Dual use research of concern     |
| <input checked="" type="checkbox"/> | <input type="checkbox"/> Plants                           |

### Methods

- |                                     |   |
|-------------------------------------|---|
| n/a                                 | Involved in the study                           |
| <input type="checkbox"/>            | <input checked="" type="checkbox"/> ChIP-seq    |
| <input checked="" type="checkbox"/> | <input type="checkbox"/> Flow cytometry         |
| <input checked="" type="checkbox"/> | <input type="checkbox"/> MRI-based neuroimaging |

## Antibodies

### Antibodies used

anti-biotin (D5A7) Rabbit mAb (Cell Signaling Technology, catalogue no. 5597S), Guinea Pig anti-Rabbit IgG secondary antibody (antibodies-online, catalogue no. ABIN101961), BG4 (scFv) was expressed as previously described (Biffi, G. et al. Nat. Chem. 5, 182–186 (2013); Hänzel-Hertsch, R. et al. Nat. Protoc. 13, 551–564 (2018)), rabbit anti-FLAG antibody (Cell Signaling Technology, catalogue no. 2368S), rabbit anti- $\gamma$ H2AX (Cell Signaling Technology, catalogue no. 2577), rabbit anti-PARP-1 (Cell Signaling Technology, catalogue no. 9532), rabbit anti- $\beta$ -Actin (Cell Signaling Technology, catalogue no. 4970).

### Validation

All commercial antibodies were validated by the manufacturers or ourselves according to a previous study. Anti-biotin (D5A7) Rabbit mAb (Cell Signaling Technology, catalogue no. 5597S) was validated by the manufacturer for Western blot and ELISA in species including human and mouse, with expected cross-reactivity across all species. Guinea Pig anti-Rabbit IgG secondary antibody (antibodies-online, catalogue no. ABIN101961) was tested for ELISA, immunohistochemistry, Western blot, CUT&RUN, and CUT&Tag in rabbit samples and preadsorbed to minimize cross-reactivity with other species. Rabbit anti-FLAG antibody (Cell Signaling Technology, catalogue no. 2368S) was validated by the manufacturer for Western Blot, immunoprecipitation, and immunofluorescence in human samples, with expected cross-reactivity across all species. Rabbit anti- $\gamma$ H2AX (Cell Signaling Technology, catalogue no. 2577) was validated for Western blot, immunofluorescence, and flow cytometry in species including human, mouse, rat, and monkey. Rabbit anti-PARP-1 (Cell Signaling Technology, catalogue no. 9532) was validated for Western blot, immunoprecipitation, and eCLIP in species including human, mouse, rat, and monkey. Rabbit anti- $\beta$ -Actin (Cell Signaling Technology, catalogue no. 4970) was validated for Western blot, immunohistochemistry, immunofluorescence, and flow cytometry in species including human, mouse, rat, monkey, bovine, and pig, and predicted to react with hamster, chicken, dog, horse, and rabbit samples based on 100% sequence homology. We validated the binding specificity and affinity of BG4 (scFv) to folded G4 DNA oligonucleotides by ELISA, as previously described (Biffi, G. et al., Nat. Chem. 5, 182–186, 2013).

## Eukaryotic cell lines

Policy information about [cell lines and Sex and Gender in Research](#)

### Cell line source(s)

Human osteosarcoma U2OS cells (HTB-96) were purchased from ATCC.

### Authentication

Short tandem repeat (STR) profiling was used to distinguish between individual human cell lines and rule out intra-species contamination. This was performed by the CRUK Cambridge Institute Biorepository Core Facility.

### Mycoplasma contamination

Cells were confirmed mycoplasma-free by periodic tests based on RNA-capture ELISA performed by the CRUK Cambridge Institute Biorepository Core Facility.

### Commonly misidentified lines (See [ICLAC](#) register)

No commonly misidentified cell lines were used.

## Plants

### Seed stocks

Report on the source of all seed stocks or other plant material used. If applicable, state the seed stock centre and catalogue number. If plant specimens were collected from the field, describe the collection location, date and sampling procedures.

### Novel plant genotypes

Describe the methods by which all novel plant genotypes were produced. This includes those generated by transgenic approaches, gene editing, chemical/radiation-based mutagenesis and hybridization. For transgenic lines, describe the transformation method, the number of independent lines analyzed and the generation upon which experiments were performed. For gene-edited lines, describe the editor used, the endogenous sequence targeted for editing, the targeting guide RNA sequence (if applicable) and how the editor was applied.

### Authentication

Describe any authentication procedures for each seed stock used or novel genotype generated. Describe any experiments used to assess the effect of a mutation and, where applicable, how potential secondary effects (e.g. second site T-DNA insertions, mosaicism, off-target gene editing) were examined.

## ChIP-seq

### Data deposition

- Confirm that both raw and final processed data have been deposited in a public database such as [GEO](#).
- Confirm that you have deposited or provided access to graph files (e.g. BED files) for the called peaks.

### Data access links

May remain private before publication.

As CUT&Tag approach displays substantially improved signal-to-noise and reduced backgrounds compared to CHIP-seq, so we performed G4-CUT&Tag and a derived method Chem-map to map endogenous folded G4 sites and binding sites of our small-molecule probe G4switch in the human genome. We also performed SLAM-seq experiments to profile the immediate effects of reversible G4 targeting by G4switch. The sequencing data generated in this study are available at the Gene Expression Omnibus (GEO) repository (<https://www.ncbi.nlm.nih.gov/geo/>) under the accession number GSE261837. The previously published GRCh38 (hg38) ([https://www.ensembl.org/Homo\\_sapiens/Info/Index](https://www.ensembl.org/Homo_sapiens/Info/Index)) and OQs (GSE110582) datasets were used.

### Files in database submission

G4switch Chem-map data files:

GSM8152791\_SLX23282\_CM\_U2OS\_G4switch400nM\_rt\_2h\_405nm.B1.t1.s350.cpm.bs3.bw  
 GSM8152792\_SLX23282\_CM\_U2OS\_G4switch400nM\_rt\_2h\_405nm.B1.t2.s350.cpm.bs3.bw  
 GSM8152793\_SLX23282\_CM\_U2OS\_G4switch400nM\_rt\_2h\_405nm.B1.t3.s350.cpm.bs3.bw  
 GSM8152794\_SLX23282\_CM\_U2OS\_G4switch400nM\_rt\_2h\_405nm.B2.t1.s350.cpm.bs3.bw  
 GSM8152795\_SLX23282\_CM\_U2OS\_G4switch400nM\_rt\_2h\_405nm.B2.t2.s350.cpm.bs3.bw  
 GSM8152796\_SLX23282\_CM\_U2OS\_G4switch400nM\_rt\_2h\_405nm.B2.t3.s350.cpm.bs3.bw  
 GSM8152797\_SLX23282\_CM\_U2OS\_G4switch400nM\_rt\_2h\_405nm.B3.t1.s350.cpm.bs3.bw  
 GSM8152798\_SLX23282\_CM\_U2OS\_G4switch400nM\_rt\_2h\_405nm.B3.t2.s350.cpm.bs3.bw  
 GSM8152799\_SLX23282\_CM\_U2OS\_G4switch400nM\_rt\_2h\_405nm.B3.t3.s350.cpm.bs3.bw  
 GSM8152800\_SLX23282\_CM\_U2OS\_G4switch400nM\_rt\_2h\_dark.B1.t1.s350.cpm.bs3.bw  
 GSM8152801\_SLX23282\_CM\_U2OS\_G4switch400nM\_rt\_2h\_dark.B1.t2.s350.cpm.bs3.bw  
 GSM8152802\_SLX23282\_CM\_U2OS\_G4switch400nM\_rt\_2h\_dark.B1.t3.s350.cpm.bs3.bw  
 GSM8152803\_SLX23282\_CM\_U2OS\_G4switch400nM\_rt\_2h\_dark.B2.t1.s350.cpm.bs3.bw  
 GSM8152804\_SLX23282\_CM\_U2OS\_G4switch400nM\_rt\_2h\_dark.B2.t2.s350.cpm.bs3.bw  
 GSM8152805\_SLX23282\_CM\_U2OS\_G4switch400nM\_rt\_2h\_dark.B2.t3.s350.cpm.bs3.bw  
 GSM8152806\_SLX23282\_CM\_U2OS\_G4switch400nM\_rt\_2h\_dark.B3.t1.s350.cpm.bs3.bw  
 GSM8152807\_SLX23282\_CM\_U2OS\_G4switch400nM\_rt\_2h\_dark.B3.t2.s350.cpm.bs3.bw  
 GSM8152808\_SLX23282\_CM\_U2OS\_G4switch400nM\_rt\_2h\_dark.B3.t3.s350.cpm.bs3.bw  
 GSM8152809\_SLX23282\_CM\_U2OS\_no1stAb\_405nm.B1.t1.s350.cpm.bs3.bw  
 GSM8152810\_SLX23282\_CM\_U2OS\_no1stAb\_405nm.B2.t1.s350.cpm.bs3.bw  
 GSM8152811\_SLX23282\_CM\_U2OS\_no1stAb\_405nm.B3.t1.s350.cpm.bs3.bw

Chem-map competition data files:

GSM8152812\_SLX23283\_CM\_U2OS\_DMSO\_3h\_G4switch400nM\_2h\_405nm.B1.t1.s350.cpm.bs3.bw  
 GSM8152813\_SLX23283\_CM\_U2OS\_DMSO\_3h\_G4switch400nM\_2h\_405nm.B2.t1.s350.cpm.bs3.bw  
 GSM8152814\_SLX23283\_CM\_U2OS\_DMSO\_3h\_G4switch400nM\_2h\_405nm.B3.t1.s350.cpm.bs3.bw  
 GSM8152815\_SLX23283\_CM\_U2OS\_PDS\_20uM\_3h\_G4switch400nM\_2h\_405nm.B1.t1.s350.cpm.bs3.bw  
 GSM8152816\_SLX23283\_CM\_U2OS\_PDS\_20uM\_3h\_G4switch400nM\_2h\_405nm.B2.t1.s350.cpm.bs3.bw  
 GSM8152817\_SLX23283\_CM\_U2OS\_PDS\_20uM\_3h\_G4switch400nM\_2h\_405nm.B3.t1.s350.cpm.bs3.bw  
 GSM8152818\_SLX23283\_CM\_U2OS\_PDS\_4uM\_3h\_G4switch400nM\_2h\_405nm.B1.t1.s350.cpm.bs3.bw  
 GSM8152819\_SLX23283\_CM\_U2OS\_PDS\_4uM\_3h\_G4switch400nM\_2h\_405nm.B2.t1.s350.cpm.bs3.bw  
 GSM8152820\_SLX23283\_CM\_U2OS\_PDS\_4uM\_3h\_G4switch400nM\_2h\_405nm.B3.t1.s350.cpm.bs3.bw

G4-CUT&Tag data files:

GSM8152786\_SLX22701\_BG4\_CnT\_U2OS\_DMSO\_noUV.B1.t1.s350.cpm.bs3.bw  
 GSM8152787\_SLX22701\_BG4\_CnT\_U2OS\_DMSO\_noUV.B1.t2.s350.cpm.bs3.bw  
 GSM8152788\_SLX22701\_BG4\_CnT\_U2OS\_DMSO\_noUV.B1.t3.s350.cpm.bs3.bw  
 GSM8152789\_SLX22701\_BG4\_CnT\_U2OS\_DMSO\_noUV.B1.t4.s350.cpm.bs3.bw  
 GSM8152790\_SLX22701\_BG4\_CnT\_U2OS\_DMSO\_noUV.B1.t5.s350.cpm.bs3.bw

SLAM-seq data files:

GSM8152766\_DMSO\_rep1\_tcount.reduced.tsv.gz  
 GSM8152766\_DMSO\_rep1\_tcount\_minus.bedgraph.gz  
 GSM8152766\_DMSO\_rep1\_tcount\_plus.bedgraph.gz

GSM8152767\_DMSO\_rep2\_tcount.reduced.tsv.gz  
 GSM8152767\_DMSO\_rep2\_tcount\_minus.bedgraph.gz  
 GSM8152767\_DMSO\_rep2\_tcount\_plus.bedgraph.gz  
 GSM8152768\_DMSO\_rep3\_tcount.reduced.tsv.gz  
 GSM8152768\_DMSO\_rep3\_tcount\_minus.bedgraph.gz  
 GSM8152768\_DMSO\_rep3\_tcount\_plus.bedgraph.gz  
 GSM8152769\_DMSO\_rep4\_tcount.reduced.tsv.gz  
 GSM8152769\_DMSO\_rep4\_tcount\_minus.bedgraph.gz  
 GSM8152769\_DMSO\_rep4\_tcount\_plus.bedgraph.gz  
 GSM8152770\_G4switch\_405nm+525nm\_rep1\_tcount.reduced.tsv.gz  
 GSM8152770\_G4switch\_405nm+525nm\_rep1\_tcount\_minus.bedgraph.gz  
 GSM8152770\_G4switch\_405nm+525nm\_rep1\_tcount\_plus.bedgraph.gz  
 GSM8152771\_G4switch\_405nm+525nm\_rep2\_tcount.reduced.tsv.gz  
 GSM8152771\_G4switch\_405nm+525nm\_rep2\_tcount\_minus.bedgraph.gz  
 GSM8152771\_G4switch\_405nm+525nm\_rep2\_tcount\_plus.bedgraph.gz  
 GSM8152772\_G4switch\_405nm+525nm\_rep3\_tcount.reduced.tsv.gz  
 GSM8152772\_G4switch\_405nm+525nm\_rep3\_tcount\_minus.bedgraph.gz  
 GSM8152772\_G4switch\_405nm+525nm\_rep3\_tcount\_plus.bedgraph.gz  
 GSM8152773\_G4switch\_405nm+525nm\_rep4\_tcount.reduced.tsv.gz  
 GSM8152773\_G4switch\_405nm+525nm\_rep4\_tcount\_minus.bedgraph.gz  
 GSM8152773\_G4switch\_405nm+525nm\_rep4\_tcount\_plus.bedgraph.gz  
 GSM8152774\_G4switch\_405nm\_rep1\_tcount.reduced.tsv.gz  
 GSM8152774\_G4switch\_405nm\_rep1\_tcount\_minus.bedgraph.gz  
 GSM8152774\_G4switch\_405nm\_rep1\_tcount\_plus.bedgraph.gz  
 GSM8152775\_G4switch\_405nm\_rep2\_tcount.reduced.tsv.gz  
 GSM8152775\_G4switch\_405nm\_rep2\_tcount\_minus.bedgraph.gz  
 GSM8152775\_G4switch\_405nm\_rep2\_tcount\_plus.bedgraph.gz  
 GSM8152776\_G4switch\_405nm\_rep3\_tcount.reduced.tsv.gz  
 GSM8152776\_G4switch\_405nm\_rep3\_tcount\_minus.bedgraph.gz  
 GSM8152776\_G4switch\_405nm\_rep3\_tcount\_plus.bedgraph.gz  
 GSM8152777\_G4switch\_405nm\_rep4\_tcount.reduced.tsv.gz  
 GSM8152777\_G4switch\_405nm\_rep4\_tcount\_minus.bedgraph.gz  
 GSM8152777\_G4switch\_405nm\_rep4\_tcount\_plus.bedgraph.gz  
 GSM8152778\_G4switch\_525nm\_rep1\_tcount.reduced.tsv.gz  
 GSM8152778\_G4switch\_525nm\_rep1\_tcount\_minus.bedgraph.gz  
 GSM8152778\_G4switch\_525nm\_rep1\_tcount\_plus.bedgraph.gz  
 GSM8152779\_G4switch\_525nm\_rep2\_tcount.reduced.tsv.gz  
 GSM8152779\_G4switch\_525nm\_rep2\_tcount\_minus.bedgraph.gz  
 GSM8152779\_G4switch\_525nm\_rep2\_tcount\_plus.bedgraph.gz  
 GSM8152780\_G4switch\_525nm\_rep3\_tcount.reduced.tsv.gz  
 GSM8152780\_G4switch\_525nm\_rep3\_tcount\_minus.bedgraph.gz  
 GSM8152780\_G4switch\_525nm\_rep3\_tcount\_plus.bedgraph.gz  
 GSM8152781\_G4switch\_525nm\_rep4\_tcount.reduced.tsv.gz  
 GSM8152781\_G4switch\_525nm\_rep4\_tcount\_minus.bedgraph.gz  
 GSM8152781\_G4switch\_525nm\_rep4\_tcount\_plus.bedgraph.gz  
 GSM8152782\_G4switch\_dark\_rep1\_tcount.reduced.tsv.gz  
 GSM8152782\_G4switch\_dark\_rep1\_tcount\_minus.bedgraph.gz  
 GSM8152782\_G4switch\_dark\_rep1\_tcount\_plus.bedgraph.gz  
 GSM8152783\_G4switch\_dark\_rep2\_tcount.reduced.tsv.gz  
 GSM8152783\_G4switch\_dark\_rep2\_tcount\_minus.bedgraph.gz  
 GSM8152783\_G4switch\_dark\_rep2\_tcount\_plus.bedgraph.gz  
 GSM8152784\_G4switch\_dark\_rep3\_tcount.reduced.tsv.gz  
 GSM8152784\_G4switch\_dark\_rep3\_tcount\_minus.bedgraph.gz  
 GSM8152784\_G4switch\_dark\_rep3\_tcount\_plus.bedgraph.gz  
 GSM8152785\_G4switch\_dark\_rep4\_tcount.reduced.tsv.gz  
 GSM8152785\_G4switch\_dark\_rep4\_tcount\_minus.bedgraph.gz  
 GSM8152785\_G4switch\_dark\_rep4\_tcount\_plus.bedgraph.gz

Genome browser session  
 (e.g. [UCSC](#))

no longer applicable

## Methodology

### Replicates

The standard Chem-map experiments were performed in three independent biological replicates each with three technical replicates (consensus peaks are defined by the overlap of the technical replicates for each biological and 2 out of 3 biological replicates for each feature).

The Chem-map competition experiments were performed in three independent biological replicates (consensus peaks are defined by the overlap of 2 out of 3 biological replicates for each feature).

The G4-CUT&Tag experiments were performed in five replicates (consensus peaks are defined by the overlap of the 3 out of 5 replicates for each feature).

The SLAM-seq experiments were performed in four independent biological replicates.

### Sequencing depth

Numbers of paired-end sequencing reads for Chem-map (61 bp read length) and G4-CUT&Tag (38 bp read length), and single-end reads for SLAM-seq (75 bp read length) are shown below in the unit of million (M):

G4switch Chem-map:

SLX23282\_CM\_U2OS\_G4switch400nM\_rt\_2h\_405nm.B1.t1, 27.7 M

SLX23282\_CM\_U2OS\_G4switch400nM\_rt\_2h\_405nm.B1.t2, 25.1 M  
 SLX23282\_CM\_U2OS\_G4switch400nM\_rt\_2h\_405nm.B1.t3, 27.4 M  
 SLX23282\_CM\_U2OS\_G4switch400nM\_rt\_2h\_405nm.B2.t1, 41.3 M  
 SLX23282\_CM\_U2OS\_G4switch400nM\_rt\_2h\_405nm.B2.t2, 23.6 M  
 SLX23282\_CM\_U2OS\_G4switch400nM\_rt\_2h\_405nm.B2.t3, 29.2 M  
 SLX23282\_CM\_U2OS\_G4switch400nM\_rt\_2h\_405nm.B3.t1, 32.9 M  
 SLX23282\_CM\_U2OS\_G4switch400nM\_rt\_2h\_405nm.B3.t2, 17.5 M  
 SLX23282\_CM\_U2OS\_G4switch400nM\_rt\_2h\_405nm.B3.t3, 33.7 M  
 SLX23282\_CM\_U2OS\_G4switch400nM\_rt\_2h\_dark.B1.t1, 26.8 M  
 SLX23282\_CM\_U2OS\_G4switch400nM\_rt\_2h\_dark.B1.t2, 33.3 M  
 SLX23282\_CM\_U2OS\_G4switch400nM\_rt\_2h\_dark.B1.t3, 22.8 M  
 SLX23282\_CM\_U2OS\_G4switch400nM\_rt\_2h\_dark.B2.t1, 26.5 M  
 SLX23282\_CM\_U2OS\_G4switch400nM\_rt\_2h\_dark.B2.t2, 33.8 M  
 SLX23282\_CM\_U2OS\_G4switch400nM\_rt\_2h\_dark.B2.t3, 27.5 M  
 SLX23282\_CM\_U2OS\_G4switch400nM\_rt\_2h\_dark.B3.t1, 21.0 M  
 SLX23282\_CM\_U2OS\_G4switch400nM\_rt\_2h\_dark.B3.t2, 35.0 M  
 SLX23282\_CM\_U2OS\_G4switch400nM\_rt\_2h\_dark.B3.t3, 31.0 M  
 SLX23282\_CM\_U2OS\_no1stAb\_405nm.B1.t1, 1.8 M  
 SLX23282\_CM\_U2OS\_no1stAb\_405nm.B2.t1, 0.9 M  
 SLX23282\_CM\_U2OS\_no1stAb\_405nm.B3.t1, 0.2 M

## Chem-map competition:

SLX23283\_CM\_U2OS\_DMSO\_3h\_G4switch400nM\_2h\_405nm.B1.t1, 24.3 M  
 SLX23283\_CM\_U2OS\_DMSO\_3h\_G4switch400nM\_2h\_405nm.B2.t1, 29.9 M  
 SLX23283\_CM\_U2OS\_DMSO\_3h\_G4switch400nM\_2h\_405nm.B3.t1, 38.3 M  
 SLX23283\_CM\_U2OS\_PDS\_20uM\_3h\_G4switch400nM\_2h\_405nm.B1.t1, 29.5 M  
 SLX23283\_CM\_U2OS\_PDS\_20uM\_3h\_G4switch400nM\_2h\_405nm.B2.t1, 25.0 M  
 SLX23283\_CM\_U2OS\_PDS\_20uM\_3h\_G4switch400nM\_2h\_405nm.B3.t1, 31.8 M  
 SLX23283\_CM\_U2OS\_PDS\_4uM\_3h\_G4switch400nM\_2h\_405nm.B1.t1, 21.9 M  
 SLX23283\_CM\_U2OS\_PDS\_4uM\_3h\_G4switch400nM\_2h\_405nm.B2.t1, 28.9 M  
 SLX23283\_CM\_U2OS\_PDS\_4uM\_3h\_G4switch400nM\_2h\_405nm.B3.t1, 26.0 M

## G4-CUT&amp;Tag:

SLX22701\_BG4\_CnT\_U2OS\_DMSO\_noUV.B1.t1, 16.5 M  
 SLX22701\_BG4\_CnT\_U2OS\_DMSO\_noUV.B1.t2, 13.2 M  
 SLX22701\_BG4\_CnT\_U2OS\_DMSO\_noUV.B1.t3, 10.9 M  
 SLX22701\_BG4\_CnT\_U2OS\_DMSO\_noUV.B1.t4, 12.0 M  
 SLX22701\_BG4\_CnT\_U2OS\_DMSO\_noUV.B1.t5, 23.6 M

## SLAM-seq:

DMSO\_dark\_rep1, 20.0 M  
 DMSO\_dark\_rep2, 20.4 M  
 DMSO\_dark\_rep3, 20.3 M  
 DMSO\_dark\_rep4, 20.7 M  
 G4switch\_dark\_rep1, 21.7 M  
 G4switch\_dark\_rep2, 20.5 M  
 G4switch\_dark\_rep3, 19.7 M  
 G4switch\_dark\_rep4, 21.8 M  
 G4switch\_405nm\_rep1, 22.0 M  
 G4switch\_405nm\_rep2, 21.7 M  
 G4switch\_405nm\_rep3, 21.0 M  
 G4switch\_405nm\_rep4, 21.3 M  
 G4switch\_405+525nm\_rep1, 19.8 M  
 G4switch\_405+525nm\_rep2, 21.1 M  
 G4switch\_405+525nm\_rep3, 21.3 M  
 G4switch\_405+525nm\_rep4, 22.2 M  
 G4switch\_525nm\_rep1, 19.7 M  
 G4switch\_525nm\_rep2, 20.2 M  
 G4switch\_525nm\_rep3, 22.4 M  
 G4switch\_525nm\_rep4, 21.6 M

## Antibodies

For each replicate, we employed:

3.4  $\mu$ l of anti-biotin (D5A7) Rabbit mAb in ~1:30 dilution against G4switch-biotin (Cell Signaling Technology, catalogue no. 5597S);  
 1  $\mu$ l of Guinea Pig anti-Rabbit IgG secondary antibody (antibodies-online, catalogue no. ABIN101961) in 1:100 dilution against anti-biotin (D5A7) Rabbit mAb;  
 ~600 nM BG4 (scFv) in 50  $\mu$ l assay buffer against endogenous folded G4 sites;  
 2  $\mu$ l of rabbit anti-FLAG antibody (Cell Signaling Technology, catalogue no. 2368S) in 1:25 dilution against BG4.

## Peak calling parameters

Peak calling parameters for Chem-map and G4-CUT&Tag experiments: ~/applications/SEACR\_1.3.sh \*bedgraph 0.01 non stringent.  
 'Slamdunk all' command parameters for SLAM-seq read mapping: : -t 5 -5 12 -n 100 -m -mv 0.2 -c 2 -rl 100

## Data quality

Individual peak numbers for q-value <0.01:

for Chem-map:

SLX23282\_CM\_U2OS\_G4switch400nM\_rt\_2h\_405nm.PCR-10.B1.t1.merged.min0.bed 15420  
 SLX23282\_CM\_U2OS\_G4switch400nM\_rt\_2h\_405nm.PCR-10.B1.t2.merged.min0.bed 15075  
 SLX23282\_CM\_U2OS\_G4switch400nM\_rt\_2h\_405nm.PCR-10.B1.t3.merged.min0.bed 15556  
 SLX23282\_CM\_U2OS\_G4switch400nM\_rt\_2h\_405nm.PCR-10.B2.t1.merged.min0.bed 18968  
 SLX23282\_CM\_U2OS\_G4switch400nM\_rt\_2h\_405nm.PCR-10.B2.t2.merged.min0.bed 16544  
 SLX23282\_CM\_U2OS\_G4switch400nM\_rt\_2h\_405nm.PCR-10.B2.t3.merged.min0.bed 16748

SLX23282\_CM\_U2OS\_G4switch400nM\_rt\_2h\_405nm.PCR-10.B3.t1.merged.min0.bed, 15586  
 SLX23282\_CM\_U2OS\_G4switch400nM\_rt\_2h\_405nm.PCR-10.B3.t2.merged.min0.bed, 14815  
 SLX23282\_CM\_U2OS\_G4switch400nM\_rt\_2h\_405nm.PCR-10.B3.t3.merged.min0.bed, 20182  
 SLX23282\_CM\_U2OS\_G4switch400nM\_rt\_2h\_dark.PCR-10.B1.t1.merged.min0.bed, 10084  
 SLX23282\_CM\_U2OS\_G4switch400nM\_rt\_2h\_dark.PCR-10.B1.t2.merged.min0.bed, 9214  
 SLX23282\_CM\_U2OS\_G4switch400nM\_rt\_2h\_dark.PCR-10.B1.t3.merged.min0.bed, 7790  
 SLX23282\_CM\_U2OS\_G4switch400nM\_rt\_2h\_dark.PCR-10.B2.t1.merged.min0.bed, 6056  
 SLX23282\_CM\_U2OS\_G4switch400nM\_rt\_2h\_dark.PCR-10.B2.t2.merged.min0.bed, 6505  
 SLX23282\_CM\_U2OS\_G4switch400nM\_rt\_2h\_dark.PCR-10.B2.t3.merged.min0.bed, 5471  
 SLX23282\_CM\_U2OS\_G4switch400nM\_rt\_2h\_dark.PCR-10.B3.t1.merged.min0.bed, 4152  
 SLX23282\_CM\_U2OS\_G4switch400nM\_rt\_2h\_dark.PCR-10.B3.t2.merged.min0.bed, 7497  
 SLX23282\_CM\_U2OS\_G4switch400nM\_rt\_2h\_dark.PCR-10.B3.t3.merged.min0.bed, 5560  
 SLX23282\_CM\_U2OS\_no1stAb\_405nm.PCR-10.B1.t1.merged.min0.bed, 2692  
 SLX23282\_CM\_U2OS\_no1stAb\_405nm.PCR-10.B2.t1.merged.min0.bed, 1193  
 SLX23282\_CM\_U2OS\_no1stAb\_405nm.PCR-10.B3.t1.merged.min0.bed, 271  
 for G4-CUT&Tag:  
 SLX22701\_bg4\_CnT\_U2OS\_DMSO\_noUV\_BG4.PCR-10.B1.t1.sortName.1000.clean.fragments.bedgraph.0.01fdr.stringent.bed, 19866  
 SLX22701\_bg4\_CnT\_U2OS\_DMSO\_noUV\_BG4.PCR-10.B1.t2.sortName.1000.clean.fragments.bedgraph.0.01fdr.stringent.bed, 17752  
 SLX22701\_bg4\_CnT\_U2OS\_DMSO\_noUV\_BG4.PCR-10.B1.t3.sortName.1000.clean.fragments.bedgraph.0.01fdr.stringent.bed, 15372  
 SLX22701\_bg4\_CnT\_U2OS\_DMSO\_noUV\_BG4.PCR-10.B1.t4.sortName.1000.clean.fragments.bedgraph.0.01fdr.stringent.bed, 16377  
 SLX22701\_bg4\_CnT\_U2OS\_DMSO\_noUV\_BG4.PCR-10.B1.t5.sortName.1000.clean.fragments.bedgraph.0.01fdr.stringent.bed, 24248

## Software

The following tools were used to analyse Chem-map, SLAM-seq, and G4-CUT&Tag data: demuxllumina (version 3.0.9), FastQC (version 0.11.8), MultiQC (version 1.11), cutadapt (version 1.18), BWA (version 0.7.17-r1188), Picard (version 2.20.3), Seacr (version 1.3), EnhancedVolcano (v.1.16.0), deepTools (version 2.0), DiffBind (version 3.10.1), Gencode v37, SlamDunk package (v.0.3.4) and DESeq2 (version 1.2.10).